



# Changes in Estuarine Sediment Dynamics with a Storm Surge Barrier

David K. Ralston<sup>1</sup>

Received: 21 June 2022 / Revised: 4 November 2022 / Accepted: 5 January 2023  
© The Author(s), under exclusive licence to Coastal and Estuarine Research Federation 2023

## Abstract

Gated storm surge barriers are increasingly being considered as part of coastal protection plans for urbanized areas located on estuaries. Barriers remain open to tidal exchange during non-storm periods, but blockage of the cross-section causes locally accelerated velocities and associated drag results in decreased tidal amplitude inside the estuary. This modeling study of a storm surge barrier near the mouth of the Hudson River estuary examines potential impacts of the alterations to flow on sediment dynamics in the system. Within about a tidal excursion of the barrier, increased bottom stresses result in erosion and coarsening of the bed. Reduced availability of fine sediment on the bed causes a reduction in suspended sediment concentration (SSC) near the barrier. Inside the estuary, reductions in tidal amplitude result in increased trapping of sediment input from the watershed due to increased stratification and a landward shift in the salinity intrusion. Despite the increased trapping, SSC in the estuary decreases due to the reduction in tidal bed stresses. Sharp velocity and stress asymmetries at the barrier openings create a divergence in sediment transport capacity that reduces export of sediment from the estuary during high discharge periods and reduces the return of sediment from offshore during low discharge. In the Hudson, the reductions in SSC (~ 10 to 20%) are modest and not expected to have major impacts on water clarity or marsh sustainability. Surge barriers may have more substantial impact on sediment dynamics in estuaries with lower background SSC or limited watershed inputs.

**Keywords** Estuary · Storm surge barrier · Sediment transport · Exchange flow · Sediment trapping

## Introduction

Gated storm surge barriers are among the shoreline protection measures being considered for many coastal cities facing increased risk of inundation with sea level rise (Mooyaart and Jonkman 2017; Nicholls et al. 2019). Surge barriers are closed temporarily during storm surge events to protect populated areas from inundation by coastal water level setup. During non-storm periods, gated openings allow for tidal exchange between the estuary and coastal ocean as well as navigation by vessels. Gated openings represent only a fraction of total width, and permanent infrastructure of the barrier blocks the rest of the estuary cross-section. The reduction in flow cross-sectional area affects tidal exchange

and can significantly alter conditions inside the estuary, potentially including the sediment dynamics.

Increased tidal velocities through the constrictions of barrier openings result in greater hydrodynamic drag due to a combination of bottom friction and form drag, and this causes a reduction in tidal amplitude inside the estuary (Nienhuis and Smaal 1994; Du et al. 2017; Ralston 2022). For example, a barrier constructed across the mouth of the Eastern Scheldt in the Netherlands in 1986 caused the tidal amplitude inside the estuary to decrease from 3.70 to 3.25 m (Nienhuis and Smaal 1994). Reductions in tidal amplitude with a barrier also affect salinity conditions in the estuary. In parts of the Eastern Scheldt, the salinity increased from about 28 to 31 psu and stratification more than doubled after the barrier, but the system remained relatively well mixed due to its large tidal range and shallow bathymetry (Bakker et al. 1990; Brand et al. 2016). Modeling studies of surge barriers for the Chesapeake and Hudson estuaries, systems that are deeper and more stratified than the Eastern Scheldt, project increases in the salinity intrusion and stratification with barriers (Du et al. 2017; Ralston 2022). Changes in

---

Communicated by Eduardo Siegle.

✉ David K. Ralston  
dralston@whoi.edu

<sup>1</sup> Woods Hole Oceanographic Institution, Woods Hole, MA, USA

the salinity dynamics in those systems are linked to reductions in tidal velocity and turbulent mixing inside the estuary and strengthening of the estuarine exchange flow. In contrast, velocity increases through the barrier openings cause increased turbulent mixing that can locally reduce the stratification and the exchange flow (Ralston 2022). Both the velocity and salinity fields illustrate differences between local impacts close to a barrier and changes farther into the estuary due to the reduction in tidal amplitude. Sediment resuspension, transport, and accumulation depend directly on tidal velocities and the salinity distribution, so correspondingly the effects of a surge barrier on sediment processes are likely to be different near the barrier and farther inside estuary.

Few studies have examined the impacts of surge barriers on estuarine sediment dynamics. As is the case more generally for surge barrier impacts, the Eastern Scheldt is the subject of the bulk of the literature on the topic. There, reductions in tidal amplitude after barrier construction resulted in reductions in tidal sediment resuspension, decreased SSC, and increased water clarity (Bakker et al. 1990; Brand et al. 2016). Reductions in tidal amplitude were also linked to changes in bed sediment composition and morphology in the estuary. Weaker tides reduced the landward sediment transport by flood-dominant currents and led to net erosion of tidal flats by wind waves, which were relatively unaffected by the barrier (de Vet et al. 2017). Tidal channels inside the estuary that were predominantly sandy before the barrier accumulated finer grained sediment, consistent with the reduction in tidal resuspension (Ten Brinke et al. 1994). Morphological changes were also observed on the ebb delta seaward of the barrier, where shoals eroded and channels experienced sedimentation, reorientation, and an overall decrease in the magnitude of sediment transport (Eelkema et al. 2013). Closer to the barrier, increased tidal velocities resulted in scour and bed erosion that was greater than anticipated (Broekema et al. 2018).

The Eastern Scheldt provides a useful case study for potential impacts of barriers, but variation in hydrodynamic or sediment transport characteristics among estuaries is also an important consideration. The Eastern Scheldt has strong tides, weak stratification, a predominantly sandy bed, and minimal watershed inputs of freshwater or fine sediment (Nienhuis and Smaal 1994; Brand et al. 2016; de Vet et al. 2017). Estuaries that have weaker tidal forcing, more substantial river inputs, or are deeper are likely to be more stratified, have stronger estuarine circulation, and have more fine sediment on the bed and in the water column (Geyer and MacCready 2014). Decreases in tidal amplitude may not only affect local resuspension, but also the location of sediment trapping at the limit of the salinity intrusion (Postma 1967; Burchard et al. 2018). Changes in net sediment transport may depend on the increases in the

strength of the estuarine circulation as well as changes to the magnitude or asymmetry of tidal currents.

The Hudson River estuary provides an example of a partially mixed estuary where sediment dynamics could be altered by construction of surge barrier. In 2012, storm surge from Hurricane Sandy resulted in a total water level that was 3.4 m above MSL (Talke et al. 2014; Orton et al. 2016), causing extensive economic damage and loss of life (Strauss et al. 2021). Risks from coastal flooding are increasing with sea level rise, with projected annualized costs for the region exceeding \$10B year<sup>-1</sup> by 2100 (US Army Corps of Engineers 2019). In light of this, the US Army Corps of Engineers has conducted feasibility studies to assess coastal protection strategies (US Army Corps of Engineers 2019). The most favorable configuration emerging from that study included a storm surge barrier located at the mouth of the Hudson between Upper and Lower New York Harbor (Fig. 1).

Potential impacts of a barrier at the mouth of the Hudson on tidal and salinity dynamics were examined in a recent modeling study (Ralston 2022). The present analysis builds on results from that study to assess alterations to the sediment dynamics from a realistic storm surge barrier. Effects of the barrier on bottom stress, suspended sediment concentration (SSC), bed composition, sediment accumulation and export, and sediment transport mechanisms are examined using idealized model simulations for a range of river discharge and tidal forcing conditions. The results inform assessment of impacts on the Hudson as well as for other partially mixed estuaries with comparable sediment dynamics.

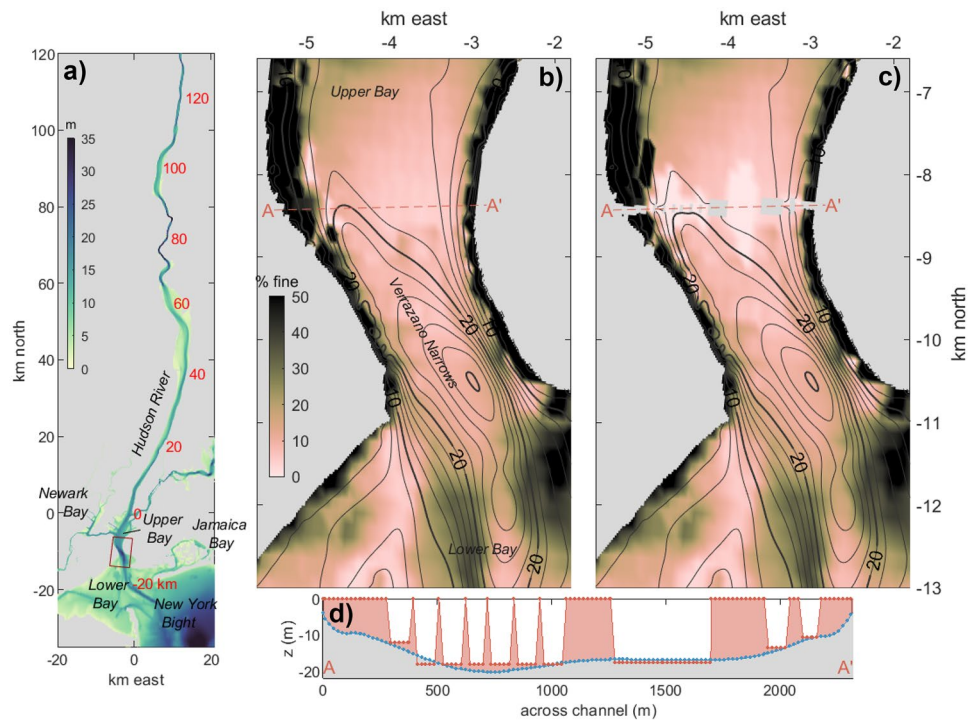
## Methods

### Hudson River Estuary

Sediment dynamics in the Hudson have been examined extensively in previous studies (Panuzio 1965; Bokuniewicz and Arnold 1984; Geyer et al. 2001; Woodruff et al. 2001). The Hudson estuary extends from New York Bight to its tidal limit near the convergence of the Mohawk and Upper Hudson Rivers at Troy NY. Together, the Mohawk and Upper Hudson have a mean discharge of 420 m<sup>3</sup> s<sup>-1</sup> and account for about 60% of the total freshwater input to the estuary, with the rest coming from smaller side tributaries (Lerczak et al. 2006; Wall et al. 2008). The total sediment discharge to the tidal Hudson averages about 1.2 Mt year<sup>-1</sup>, and about half of that comes from the Mohawk and Upper Hudson (Ralston et al. 2021).

The Hudson is a partially mixed estuary where stratification and the salinity intrusion vary with tidal amplitude and river discharge (Abood 1974; Ralston et al. 2008). Tides at the mouth have a mean range of about 1.5 m and

**Fig. 1** Model bathymetry. **a** Lower Hudson River and New York Harbor in outer grid; the full grid extends north to the tidal limit of the Hudson and includes regions to the east (Western Long Island Sound) and west (Newark Bay, Arthur Kill). Distance from The Battery (km) and location of the nest zoom are marked in red. **b** Zoom on center of nest grid at Verrazano Narrows for base case. Color shows fractional mud in the bed initial condition and contours mark depth. A-A' indicates the cross-section in the lower panel. **c** Zoom on the nested grid for the barrier case. **d** Cross-section at barrier location with grid cell depths for the base case (blue markers) and barrier case (red markers)



a spring-neap tidal range of 2.0 to 0.5 m. The estuary is oriented approximately north–south. Distances along the estuary are reported from The Battery at the southern tip of Manhattan, although the mouth of the estuary is about 20 km south at Ambrose Bar. The distance along-estuary following the thalweg and the straight-line distance north from the Battery are similar (Fig. 1), so for simplicity the latter are used in the results presented here. During the spring freshet, the combined river discharge is often in the range of 2000–4000  $\text{m}^3\text{s}^{-1}$  and the salinity intrusion on average is around 40 km north of The Battery. During the late summer, discharge can decrease to 100–200  $\text{m}^3\text{s}^{-1}$  for extended periods and the salinity intrusion moves landward more than 100 km. The salinity intrusion shifts landward during neap tides and seaward during spring tides with the respective increase and decrease in the strength of the estuarine circulation. Spring-neap variation is amplified during high discharge periods compared with its more muted response for low discharge conditions (Ralston et al. 2008).

Suspended sediment concentrations in the estuary vary seasonally in magnitude and spatial distribution. The primary estuary turbidity maximum (ETM) is located 10–30 km from the Battery, centered near the constriction at the George Washington Bridge (Geyer et al. 2001). During the spring freshet, SSC in the ETM can exceed 1000  $\text{mg L}^{-1}$  and short-term bed sediment accumulation rates can equal 10 s of  $\text{cm year}^{-1}$  (Feng et al. 1998; Woodruff et al. 2001; Traykovski et al. 2004). During lower discharge periods, a secondary ETM is found in Haverstraw Bay around 60 km north

(Bokuniewicz and Arnold 1984). Maximum near-bottom sediment concentrations in the upper ETM are around 500  $\text{mg L}^{-1}$  and the region is highly depositional (Nitsche et al. 2010; Ralston et al. 2012). Long-term accumulation rates in the Hudson are consistent with the local rate of sea level rise of about 3  $\text{mm year}^{-1}$  (Olsen et al. 1978; Klingbeil and Sommerfield 2005; Slagle et al. 2006), although short-term rates can be significantly greater (Sommerfield 2006).

## Model Setup

The research approach uses a hydrodynamic and sediment transport model to assess changes in conditions resulting from realistic storm surge barrier near the mouth of the estuary. The model grid and forcing are the same as was used to assess effects of the barrier on tidal and salinity dynamics (Ralston 2022). The circulation model is the Regional Ocean Modeling System (ROMS) (Shchepetkin and McWilliams 2005; Haidvogel et al. 2008). A nested grid is used to increase resolution near the barrier (Fig. 1). The outer grid includes the tidal Hudson River and New York Harbor, and it has open boundaries in New York Bight and western Long Island Sound. The along-estuary grid resolution of the outer grid is 100–200 m, and across-estuary grid resolution is 50–100 m. A nested, inner grid focuses on the Verrazano Narrows region and has 5 times the horizontal resolution of the outer grid: 25–30 m along-estuary and 20 m across-estuary. The model has 16 terrain-following, uniformly spaced layers in

the vertical. Additional details on the circulation model are provided in Ralston (2022).

Sediment transport is integrated with ROMS with the Community Sediment Transport Model (Warner et al. 2008). The setup of the sediment transport model is the same as in previous studies of the Hudson that included comparisons with observations (Ralston et al. 2012; Ralston et al. 2013; Ralston and Geyer 2017; Chant et al. 2021). Multiple sediment size classes are represented, and new sediment inputs with river discharge are tracked separately from sediment initially on the bed. The initial conditions for the bed are derived from observations of bed composition using sidescan sonar and grab sampling (Nitsche et al. 2007). Bed sediment is divided into three size classes: medium sand (settling velocity  $w_s=40 \text{ mm s}^{-1}$ ; critical stress for erosion  $\tau_{ce}=0.5 \text{ N m}^{-2}$ ), fine sand ( $w_s=5 \text{ mm s}^{-1}$ ;  $\tau_{ce}=0.1 \text{ N m}^{-2}$ ), and medium silt ( $w_s=0.6 \text{ mm s}^{-1}$ ;  $\tau_{ce}=0.05 \text{ N m}^{-2}$ ). New sediment inputs with river discharge are divided into two size classes: fine silt ( $w_s=0.2 \text{ mm s}^{-1}$ ;  $\tau_{ce}=0.05 \text{ N m}^{-2}$ , 80% of river input) and very fine silt ( $w_s=0.01 \text{ mm s}^{-1}$ ;  $\tau_{ce}=0.05 \text{ N m}^{-2}$ , 20%). The slower settling river sediment is representative of washload and particularly affects the total SSC during high discharge events (Ralston et al. 2013). The two river sediment classes are a crude representation of the continuous distribution of particle sizes in the real world, but the approach has been effective in comparisons with observations and is useful for assessing the influence of settling velocity on transport processes. Sediment in the model is non-cohesive and so it does not represent flocculation or transport processes at long-time scales. Watershed sediment inputs that are retained in the estuary for extended periods interact with other sediment and organic matter to form faster-settling flocs. The flocculated fine sediments found in the saline estuary are represented in the model by the “medium silt” settling velocity of the bed (Traykovski et al. 2004). Despite the simplifications, the settling velocity size classes have proven useful in comparisons with suspended sediment observations at event to seasonal time scales (Ralston et al. 2012, 2013; Ralston and Geyer 2017).

The model is run in two bathymetric configurations: a baseline representing present conditions and a storm surge barrier case. The surge barrier is based on a conceptual design in the New York–New Jersey Harbor and Tributaries (NYNJHAT) Coastal Storm Risk Management Feasibility Study Interim Report (US Army Corps of Engineers 2019). That study examined multiple potential approaches for storm surge mitigation including different barrier configurations and shoreline protection measures. The configuration here is a surge barrier located north of Verrazano Narrows between Upper and Lower New York Bays (Fig. 1). The flow cross-section in the model grid is blocked at locations where there would be permanent infrastructure housing the navigational and tidal flow gates in the conceptual design. The total cross-section remaining open to flow in the model grid

(58.3%) is similar to that in the conceptual design (58.5%) (US Army Corps of Engineers 2019; Ralston 2022).

The model is run with idealized forcing to assess the influence of the barrier on sediment dynamics over a range of conditions. Tidal forcing at the open boundaries is simplified to the three largest components (M2, S2, and N2) to retain monthly asymmetry in the spring-neap cycle, but the total tidal amplitude comparable to the full set of tidal constituents. Constant river discharge cases are run across the seasonal range: 125, 500, and 2000  $\text{m}^3 \text{ s}^{-1}$ , which represent low (5th percentile), average (50th percentile), and high discharge conditions (98th percentile). Suspended sediment concentration in the river discharge is based on rating curves from observations (Ralston et al. 2021). For both the baseline and barrier cases, the bed sediment distribution is allowed to adjust over a spin-up period of 2 months to reduce the influence of transients from the initial condition. This spin-up primarily influences the bed near the barrier, where high velocities through barrier openings erode fine sediment and coarsen the bed relative to the base case (Fig. 1). The bed is then re-initialized with the size class distribution from the end of the spin-up and a uniform thickness of 30 cm. This initial bed thickness is sufficient such that it does not limit sediment availability for erosion over the simulation period. Each of the six scenarios (with and without a barrier, three constant discharges) is then run for about 2 months (55 days) to cover the range of tidal forcing and establish quasi-steady state distributions of salinity and SSC.

## Results

Constriction of the tidal flow through barrier openings causes alterations to conditions both near the barrier and farther inside the estuary, and the response often changes with distance from the barrier. For example, depth-averaged tidal velocities in the barrier openings increase by about a factor of 2 with the reduction in cross-sectional area, but farther inside the estuary tidal velocities decrease by 5–10% due to loss of tidal energy from the drag at the barrier (Ralston 2022). Similarly, stronger tidal velocities cause increased mixing and reductions in stratification near the barriers, but farther inside the estuary, weaker tides result in reductions in mixing and increased stratification. Tidal velocities play a central role in sediment transport, so the alterations to the suspended and bed sediment conditions vary with distance from the barrier.

For illustration, time series of mean bottom stress and near-bed suspended sediment concentration are averaged over regions near the barrier and in the lower ETM (Fig. 2). In both regions, bottom stress and SSC vary by more than a factor of 2 over the spring-neap cycle. Near the barrier, the average bottom stresses increase by about 40% compared

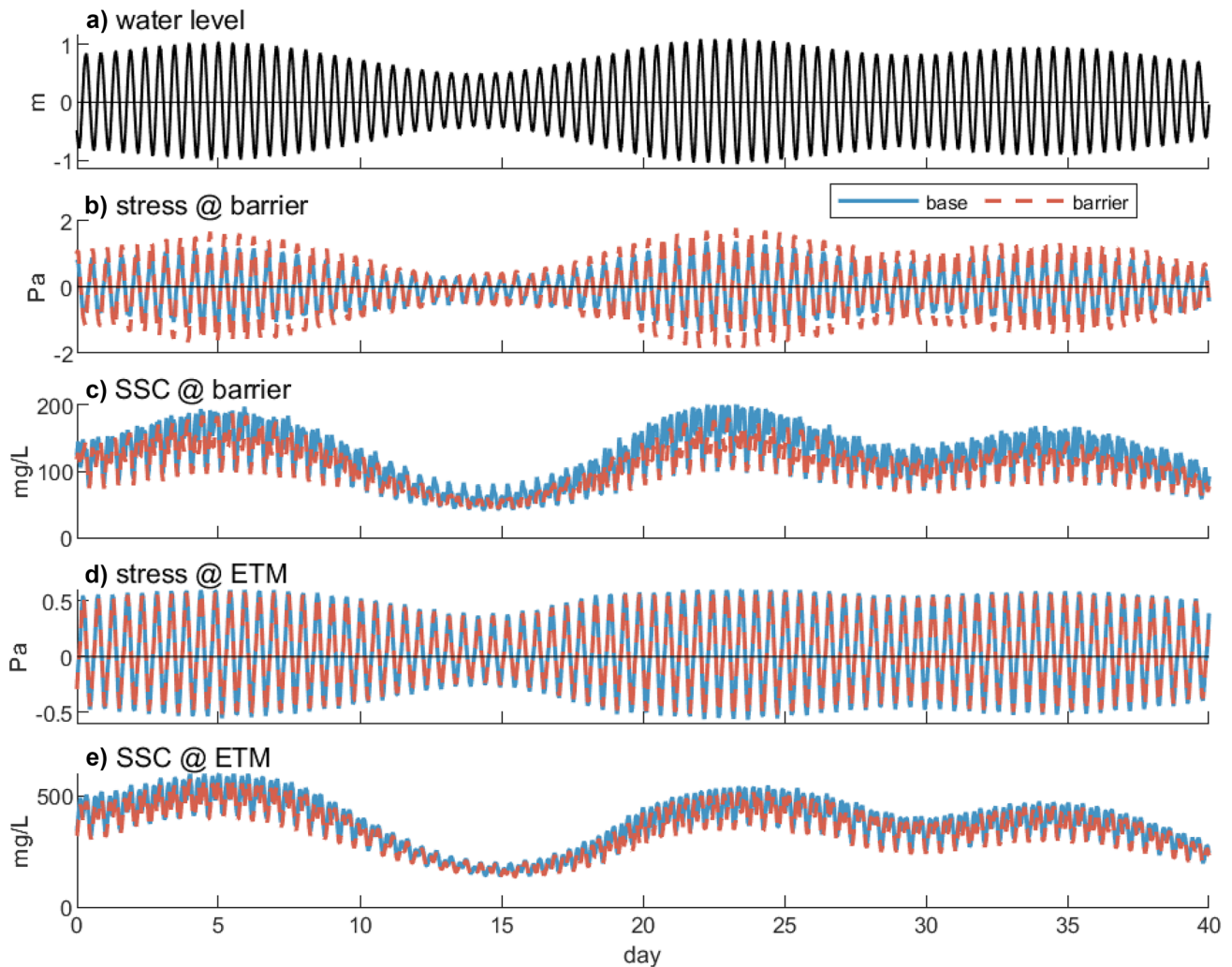


**Fig. 2** Time series of conditions near the barrier and in the lower Hudson estuarine turbidity maximum (ETM) for the moderate discharge case. **a** Spring-neap variations in water level during the simulation

period. **b** Laterally averaged bottom stress and **c** suspended sediment concentration near the barrier (−9 to −7.5 km north); **d** laterally averaged bottom stress and **e** in the lower Hudson ETM (15 to 25 km north)

with the base case over most of the simulation period. The increase in bottom stress is greater during flood tides (40–50%) than during ebbs (30–40%). The differences in stress are less pronounced during the weakest neap tides (days 12–16) than other tidal conditions. Average SSC near the barrier decreases moderately (10–20%) with the barrier despite the overall increase in bottom stress. This reduction in SSC results from the reduction in the availability of fine-grained bed sediment for resuspension in the barrier case.

In contrast, both bottom stress and SSC decrease in the ETM with the barrier compared to the base case. Suspended sediment concentrations are much greater in the ETM region than near the barrier due to the differences in bed sediment composition and sediment trapping. Decreases in average bottom stress in the ETM are 5–10% due to the decrease in tidal amplitude with the barrier.

Fractional decreases in tidal maximum SSC in the ETM region are similar to the stress at around 5–10%.

The selected time series highlight the spatial differences in sediment response between the region near the barrier (increased bottom stress, decreased SSC) and the rest of the estuary (decreased stress, decreased SSC). The subsequent results are organized according to this spatial gradient, recognizing that the changes in conditions with distance from the barrier occur along a continuum and vary with river discharge, tidal forcing, and sediment characteristics.

### Stress, Suspended Sediment, and Bed Composition Near the Barrier

The obstruction of the tidal flow by the surge barrier piers causes increased tidal velocities, with jets of higher velocity

emanating from the barrier openings (Fig. 3). The velocity field near the barrier is tidally asymmetric, with enhanced flood-oriented velocities landward of the openings during flood tides and ebb-oriented velocities seaward of the openings during ebbs. Correspondingly, the bottom stress near the barrier is sharply asymmetric. The high velocities through the openings cause flow separation downstream of the barrier piers, and in the separation zones the tidal flow is weakened or reversed (Ralston 2022). The flow separation causes eddy shedding, and the near-bottom SSC distribution reflects the

velocity structure of the eddies due to local enhancement of the bottom stress and resuspension (Fig. 3). Near-bottom sediment concentrations are also enhanced in the centers of the eddies where the flow converges and decelerates. The lateral gradients in near-bottom SSC also depend on the bed composition, with predominantly sand in the middle of the channel and finer sediment on the lateral shoals (Fig. 1). Fine sediment supply from the bed is limited other than at the edges of the channel, and thus the SSC distribution does not necessarily correspond with the velocity or bottom stress distribution.

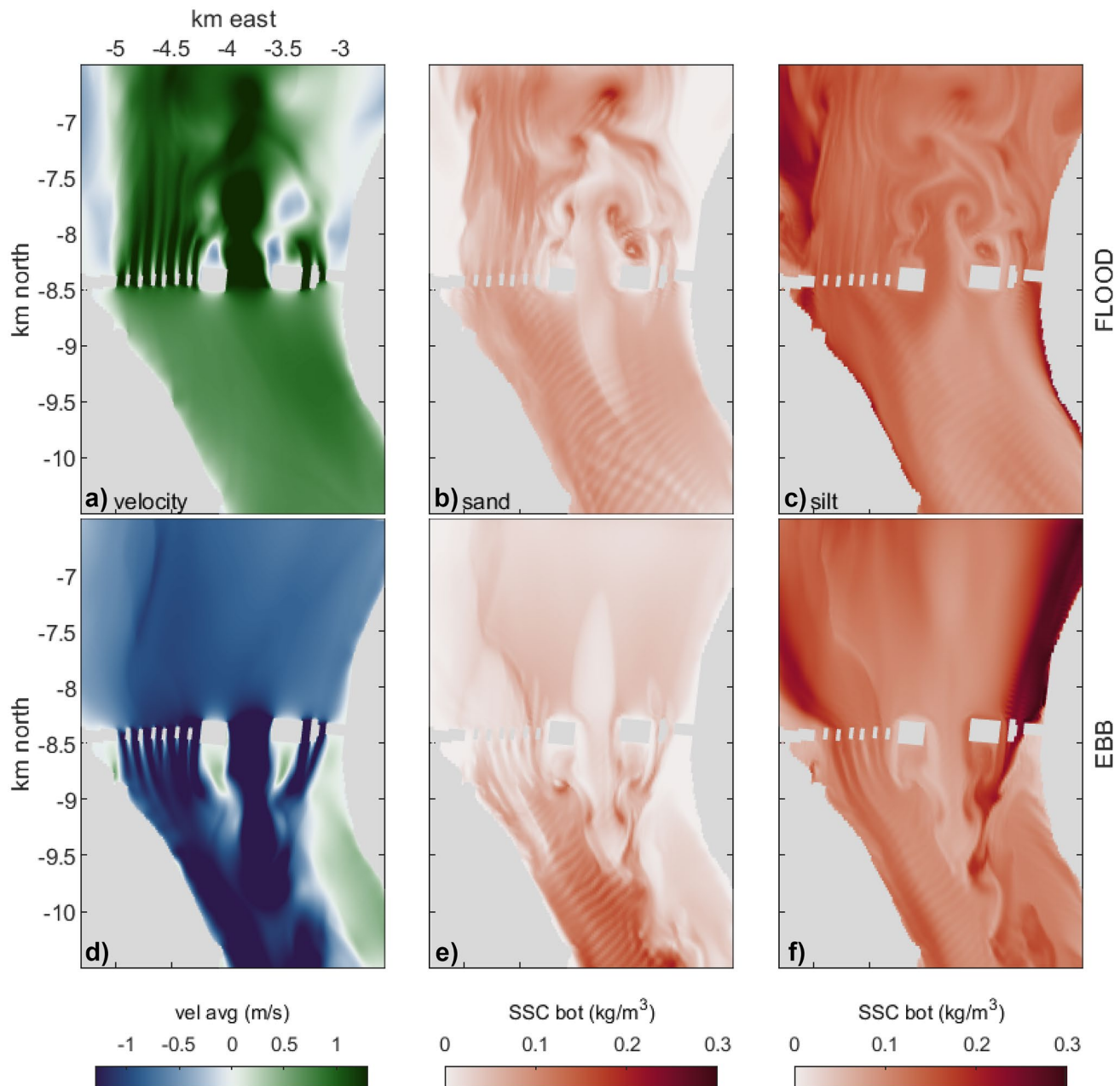


**Fig. 3** Spring tide conditions (day 22, see Fig. 2) near the barrier for the moderate discharge case during **a–c** flood tide and **d–f** ebb tide. **a, d** Northward depth-averaged velocity; **b, e** near-bed suspended sediment concentration (SSC) of sand; **c, f** near-bed SSC of fine sediment

The presence of the barrier induces tidal asymmetry in the resuspension by altering the flow patterns. For example, on the relatively muddy eastern shoal resuspension is greater seaward of the barrier during flood tides and greater landward of the barrier during ebbs. During both phases of the tide, the barrier piers enhance the flow separation that results from the channel curvature and thereby expand the shadow zone of low velocity and low SSC on the eastern shoals downstream of the barrier. In contrast, the velocity and SSC distributions in the base case vary smoothly and do not exhibit strong tidal asymmetries in magnitude and structure (see Supplementary Material). The example (Fig. 3) is for spring tides when velocities and flow separation at the barrier are strongest and the differences between the base and barrier cases are most pronounced.

Bottom stress directly affects sediment resuspension and near-bed SSC, so tidal asymmetries in velocity near the

barrier openings impact the net sediment transport. In the base case, mean bottom stress is flood-dominant in the deep, central part of the channel and mean stress is ebb dominant on the lateral shoals (Fig. 4a). Note that bottom stress has the opposite sign as the near-bottom velocity, so bottom stress during flood tide is negative. This lateral stress distribution is consistent with results from elsewhere in the estuary where sediment transport is predominantly landward in the deep channel and seaward on the shoals due to the increasing influence of the estuarine circulation with water depth (Ralston and Geyer 2009; Ralston et al. 2012). Note also there is asymmetry in transport associated with flow curvature on the east side of the channel, where flow separation near the bed apex causes a change in sign of the mean stress. In the barrier case, this stress asymmetry is shifted landward from the bend apex to the barrier and it expands out into the

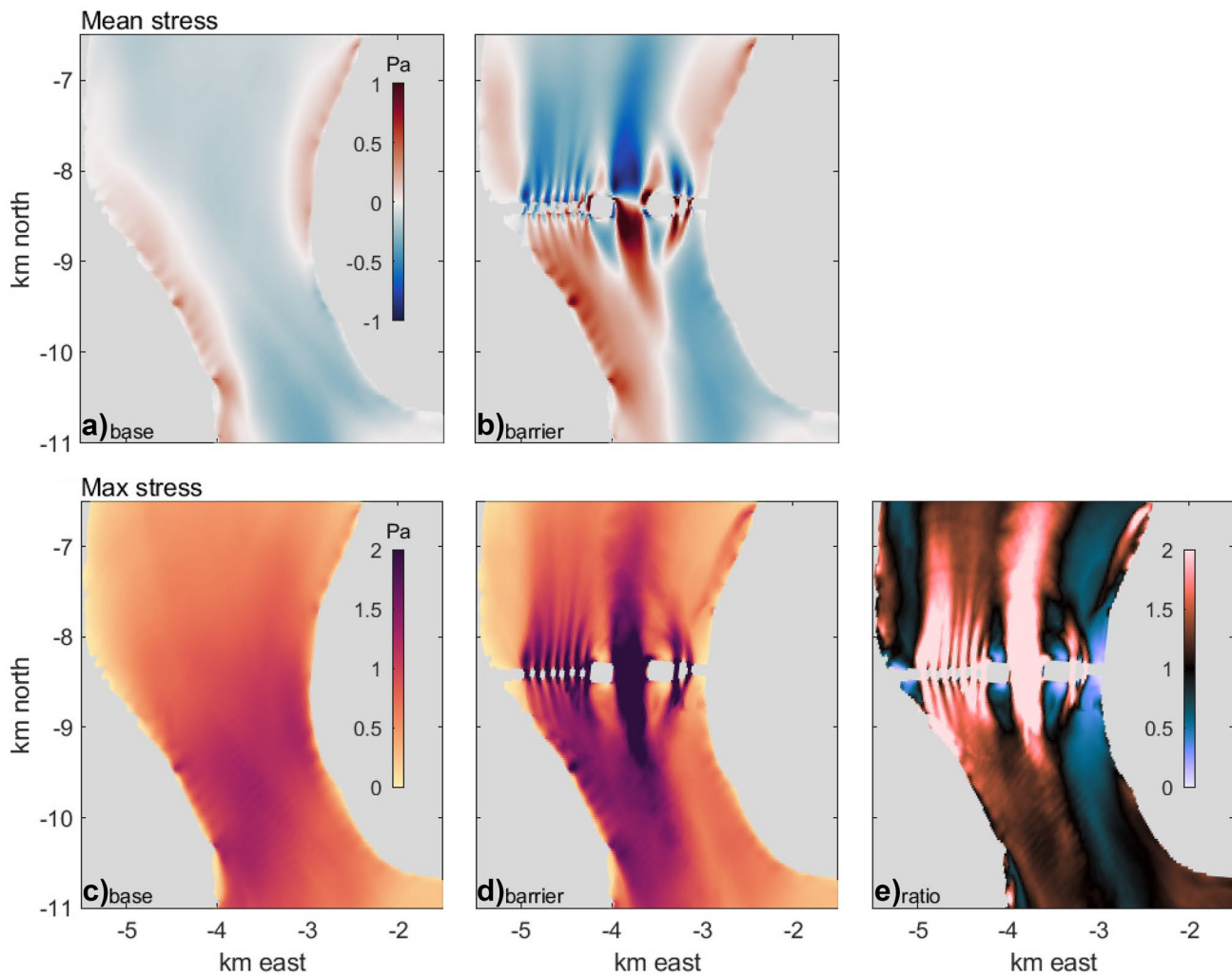


**Fig. 4** Mean bottom stress (upper panels) and maximum bottom stress amplitude (lower panels) near the barrier for the  $500 \text{ m}^3\text{s}^{-1}$  discharge case averaged over the simulation period (55 days). **a** Mean bottom stress

in base case; **b** mean bottom stress with barrier. **d** Maximum stress in base case; **e** maximum stress with barrier; **f** ratio of maximum stresses

channel (Fig. 4b)). The barrier marks a distinct separation between strongly flood-oriented mean stresses landward of the barrier and strongly ebb-oriented stresses seaward of the openings. This sharp divergence in mean stress at the barrier openings indicates the potential for divergence in sediment transport, depending on sediment availability. The opposite is the case adjacent to the barrier piers where mean stresses are oriented toward the piers due to the flow separation and recirculation, indicating the potential for sediment convergence and accumulation near the piers.

The effect of the barrier on mean bottom stress varies with river discharge. Considering the laterally averaged bottom stress, the distance over which the barrier alters the flow varies inversely with river discharge (Fig. 5a–c)). For the low discharge case, landward stresses with the barrier increase more than 5 km into the estuary, whereas for

high discharge the influence on the mean stress diminishes around 2 km from the barrier. In both the base and barrier cases, increasing river discharge increases the stratification and the estuarine exchange flow, and thus enhances the landward bottom stress (Ralston 2022). Close to the barrier, strong flood velocities through the barrier openings add to the mean landward stress from the estuarine circulation. Similarly for the ebb currents and seaward of the barrier, the offset in mean bottom stress between the base and barrier cases extends farther seaward in the low discharge case than the high discharge case. Strong velocities through the barrier openings locally increase the turbulent mixing and shift the mean stresses seaward, but the greater stratification in the high discharge case dampens alterations to the mean stress compared with the low discharge case.

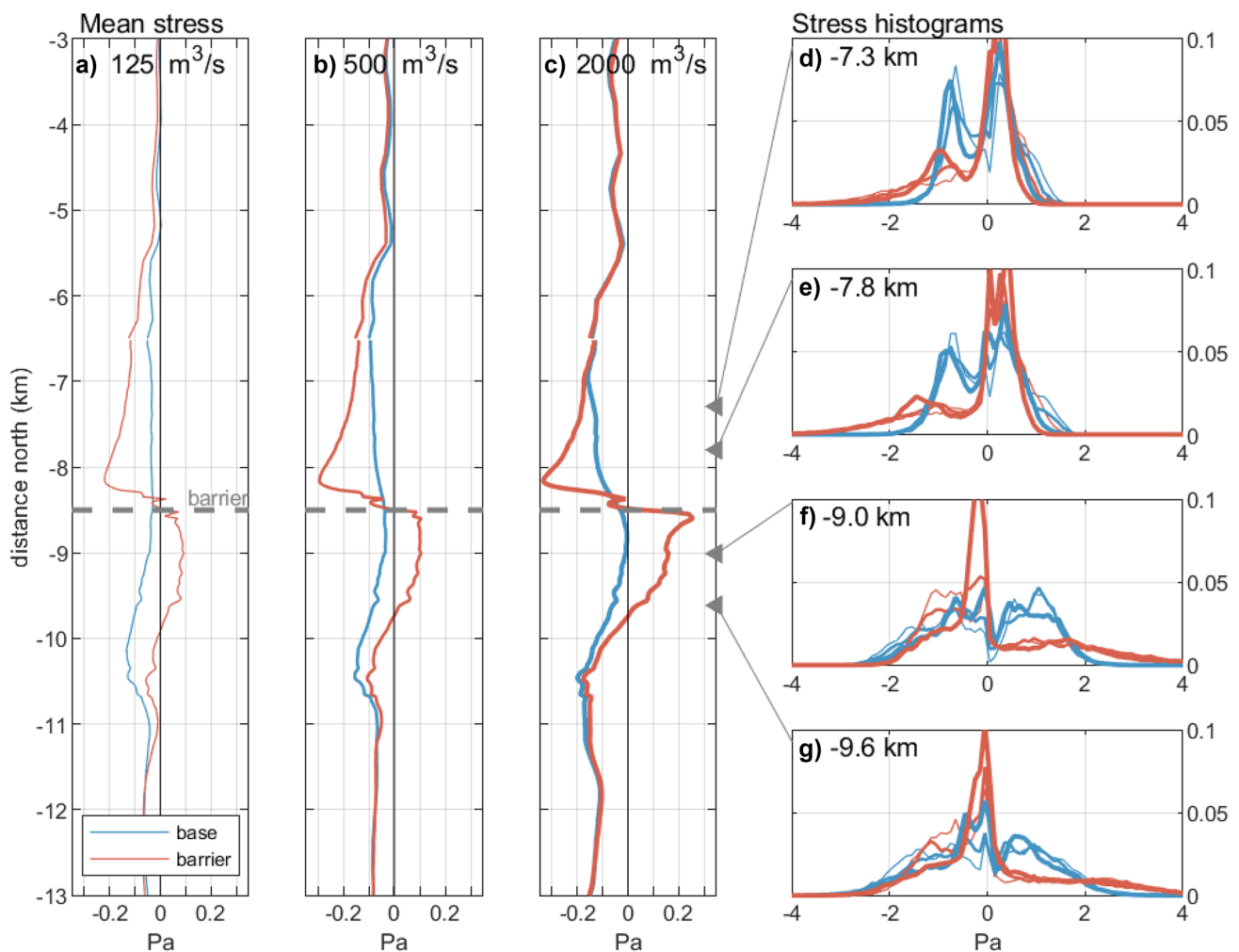


**Fig. 5** Mean bottom stress near the barrier location. Left panels: laterally averaged bottom stress for the base and barrier cases with river discharge of **a**  $125 \text{ m}^3\text{s}^{-1}$ , **b**  $500 \text{ m}^3\text{s}^{-1}$ , and **c**  $2000 \text{ m}^3\text{s}^{-1}$ , averaged over the simulation period (55 days). Right panels: histograms of bot-

tom stress at locations **d**, **e** landward and **f**, **g** seaward of the barrier. Histograms for the base and barrier cases are shown for the three discharge conditions

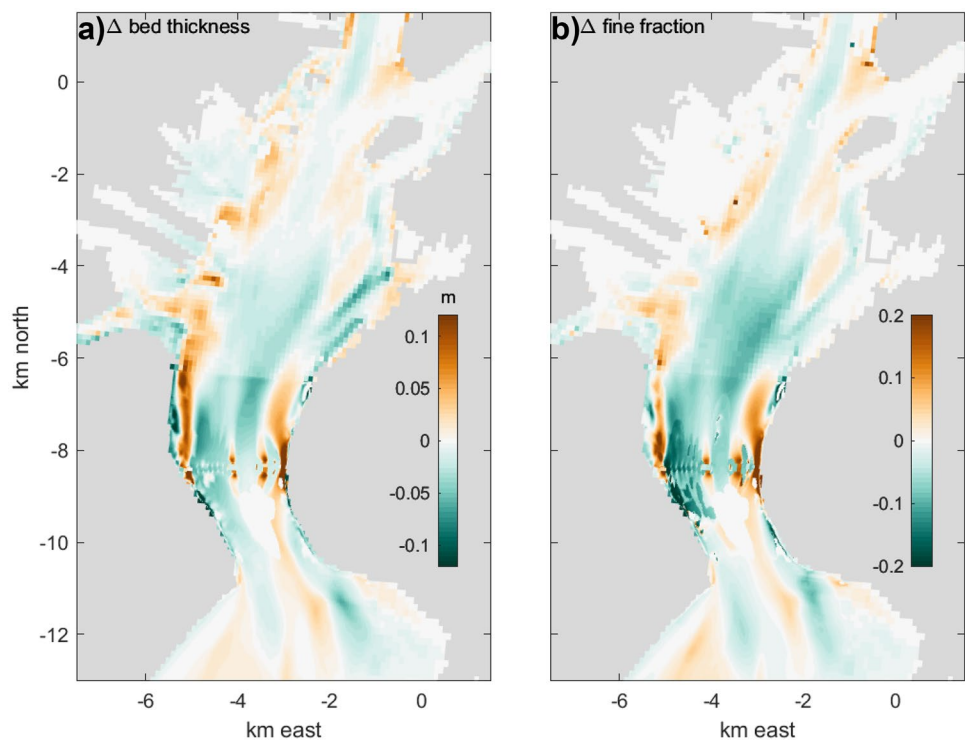
Mean stresses can be indicative of the direction of net sediment transport, but the instantaneous tidal stresses greatly exceed the mean values and directly affect sediment resuspension. In the model, the formulation for erosion from the bed is proportional to the excess shear stress above a critical threshold (Ariathurai and Arulanandan 1978; Warner et al. 2008). Histograms of laterally averaged bottom stress are shown for cross-sections landward and seaward of the barrier (Fig. 5). In the base case, the stress distributions are relatively symmetric in all the cross-sections, and maximum stresses are typically less than 2 Pa. With the barrier, the amplitude of the maximum stresses increases to about 3 Pa in the cross-sections landward of the barrier during flood tides, and the amplitude reaches 4 Pa seaward of the barrier during ebb tides. The stress distributions shift toward lower amplitude during the opposite phase of the tide, so tidal stresses are reduced on average in the cross-sections landward of the barrier during ebbs and stresses are reduced seaward of the barrier during ebb. The shifts in the stress distributions result from the asymmetry in the tidally reversing jet-sink flow through the barrier openings.

Map views of the distributions of the maximum stress with and without the barrier illustrate the effect of flow through openings (Fig. 4). In the base case, maximum stresses occur in the deepest part of the constriction at Verrazano Narrows, and over most of the region the maximum stresses are around 1 Pa (Fig. 4c)). With the barrier, the maximum tidal stresses occur in the openings and are greater than 2 Pa over large areas (Fig. 4d)). The ratio of

the maximum tidal stresses with the barrier to the base case correspond with the alterations to the tidal currents (Fig. 3). Bottom stresses increase in regions influenced by the velocity jets through the openings and stresses decrease in separation zones near the piers. Several km away from the barrier the maximum stresses increase by a factor of 1.5 more, and the increase exceeds a factor of 2 close to the barrier.

The changes in the bottom stress with the barrier broadly correspond with changes in bed sediment thickness and composition (Fig. 6). Regions of erosion and net decrease in sediment bed sediment thickness are located landward and seaward of the barrier openings and extend into the middle of the Upper Bay. Sediment accumulates on the lateral shoals, particularly landward of the barrier and on the west side of the Upper Bay. Differences in bed sediment composition reflect the differences in erosion and deposition, with accumulation of fine sediment in depositional areas and loss of fine sediment in erosional areas. Near the barrier openings and in the deep, central parts of Upper Bay the bed sediment coarsens. On the shoals landward of the barrier piers and on the west side of the bay the fine fraction in the bed increases. The spatial patterns of erosion and coarsening are consistent with increased stresses causing increase resuspension of fine sediment up to several km from the barrier openings. Some of this fine sediment deposits in lower stress regions at the edges of the estuary and in flow separation zones near the barrier piers. The example shown is for the moderate discharge of  $500 \text{ m}^3 \text{ s}^{-1}$ , but the spatial patterns of erosion and deposition are similar for the other

**Fig. 6** Differences in bed composition between the base and barrier cases for  $Q_r = 500 \text{ m}^3 \text{ s}^{-1}$ . **a** Difference in bed thickness; **b** difference in fine sediment fraction in the bed



discharge cases. In the low discharge case, the region of erosion and coarsening extends farther landward into the Upper Bay, whereas in the high discharge case the region of fine sediment accumulation is more extensive on the west side of the Upper Bay (not shown). The greater landward extent of the changes in bed thickness and composition for the low discharge case results from the more extensive alteration to the flood-dominant bottom stresses (Fig. 5).

### Sediment Distribution and Retention in the Estuary

Stronger tidal flows through barrier openings locally increase bottom stress amplitudes and cause erosion and coarsening of the bed in the main channel. Farther landward, tidal velocities are weaker with the barrier than in the base case, which reduces the tidal stresses, shifts the salinity distribution landward, and increases stratification (Ralston 2022). The presence of the barrier alters both the amplitude of the tidal stresses and the mean bottom stress. Reductions in tidal velocity cause an overall reduction in bottom stress amplitude, and greater stratification reduces the eddy viscosity and decreases the bottom stress for a given depth-averaged velocity. For example, in the  $500 \text{ m}^3\text{s}^{-1}$  case the magnitude of the bottom stress in the lower Hudson (e.g., 0–40 km) with the barrier decreases by 5–10% compared with the base (Fig. 7a)). Decreases in the magnitude of the tidal velocity, and correspondingly the magnitude of the tidal bottom stress, are similar for the low and high discharge cases.

The mean bottom stress depends on asymmetries between flood and ebb velocities, which are shifted to be more flood-oriented in the estuary with the barrier. Weaker tides and decreased mixing allow for stronger estuarine circulation and enhanced landward-oriented near-bottom velocities (Ralston 2022). The extent of influence of the increased estuarine circulation depends on the location of the salinity intrusion, which varies inversely with river discharge. For the low discharge case, the mean stress is consistent with mean landward near-bottom velocity up to the limit of the salinity intrusion around 110 km north, and the mean stress becomes more landward with the barrier than without it (Fig. 7b)). For the higher discharge cases, the transition from landward-oriented mean bottom stress in the estuary to seaward-oriented stress in the tidal river occurs near the salinity intrusion limit, and the mean stresses are shifted to be more landward within the salinity intrusion with the barrier (Fig. 7c–d)).

The reduction in tidal stress amplitude and landward shift in the mean stress results in increased trapping of new sediment input with the river discharge (Fig. 7). The along-estuary distribution of the river sediment depends on the discharge and the location of the salinity intrusion, as well as on along-estuary bathymetry that affects frontal formation and

localized sediment trapping (Ralston et al. 2012). The laterally integrated mass of new sediment is greater with the barrier than without it, particularly within the salinity gradient. For the low discharge case, the enhanced trapping extends landward more than 100 km, whereas for the high discharge case the enhanced trapping is restricted to the lower 50 km, corresponding with the location of the salinity intrusion for each. In all discharge cases, more river sediment is retained in the lower Hudson ETM (centered around 20 km) with the barrier than without. Farther seaward, less river sediment accumulates with the barrier for all the discharge cases, which is consistent with the overall increase in erosion and coarsening of the bed in the Upper Bay (Fig. 6).

The increased mobilization of bed sediment (Fig. 6) near the barrier and the trapping of river inputs farther landward (Fig. 7) affect the sediment distribution along the estuary and the export of sediment to the coastal zone. Differences in sediment mass between the base and barrier cases are grouped by region for the three discharge cases (Fig. 8). Considering all fine sediment (initial bed plus river inputs), the biggest difference with the barrier is the loss of sediment from the Upper Bay. This primarily represents bed material eroded by the increased bottom stress, and it is redistributed both landward to the lower Hudson and seaward to the Lower Bay. In contrast, new river inputs are retained more in the Hudson with the barrier, and this corresponds with a reduction in delivery of new sediment to regions farther seaward (Fig. 8). The river inputs are retained both in the tidal river and the saline estuary, which is defined here as up to 120 km north. Transport of new river sediment beyond the barrier and accumulation in the Lower Bay and New York Bight regions are reduced. The fractional reductions in sediment export are greatest in the low discharge case, but the mass of sediment delivered offshore increases with discharge, so the magnitude of sediment export is most affected in the high discharge case. New sediment inputs also accumulate less in the Upper Bay due to the increased tidal velocities that enhance scour and limit deposition in this region.

Changes in SSC along the estuary depend on a combination of factors including the changes in bottom stress and the sediment mass distribution along the estuary. An example from spring tides in the moderate discharge case illustrates the contributing factors (Fig. 9). Near-bottom SSC is maximum on the western shoals in the ETM, and SSC decreases farther seaward (Fig. 9a). With the barrier, SSC decreases compared to the base case in most of the estuary (Fig. 9b). The decreases in SSC during spring tides are typically in the range of  $20\text{--}100 \text{ mg L}^{-1}$ , and fractionally represent changes of around 15–30% near the barrier and around 5–10% in the ETM. The decrease in SSC near the barrier is due to loss of fine sediment in the bed available for resuspension, whereas farther into the estuary the reduction

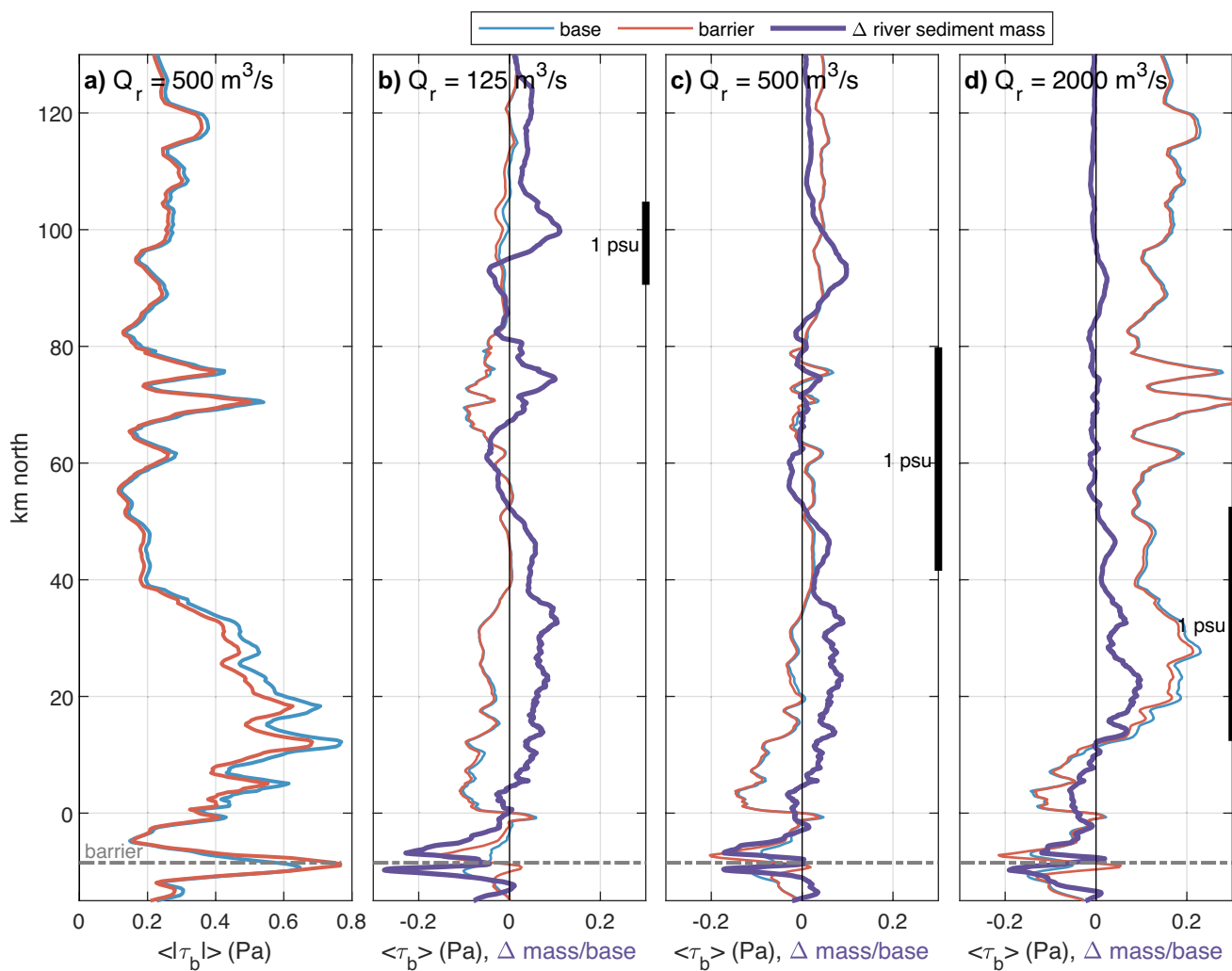


**Fig. 7** Along-estuary distributions of bottom stress and sediment mass at the end of the simulation period. **a** Mean bottom stress amplitude for the base and barrier cases for  $Q_r = 500 \text{ m}^3\text{s}^{-1}$  averaged over the simulation period (55 days). **b–d** Mean bottom stress for the base

and barrier cases and the fractional difference in sediment mass input with the river discharge for  $Q_r = 125$  (**b**),  $500$  (**c**), and  $2000 \text{ m}^3\text{s}^{-1}$  (**d**). Noted on the right axis for each discharge case is the range of the 1 psu isohaline of bottom salinity

in SSC is because of weaker tidal velocities and reduced bottom stresses. Considering only new sediment input from the river, enhanced trapping with the barrier results in regions of increased sediment resuspension (Fig. 9c–d). This new sediment represents only a small fraction of the total sediment in suspension including bed material, so while the concentration of new sediment in the water column increases, the total SSC decreases. The faster-settling size class of river sediment accumulates and is resuspended predominantly in the ETM, whereas the slower settling class is transported farther downstream in resuspended in the Upper and Lower Bay near the barrier.

Changes in SSC with the barrier also depend on the salinity distribution through its influence on the estuarine circulation and stratification, and thus vary with river discharge and tidal amplitude (Fig. 10). Near the barrier,

increased mixing reduces stratification and causes a reduction in near-bottom salinity. Inside the estuary, the reduction in tidal amplitude causes an increase in the length of the salinity intrusion and an increase in stratification. The landward shift in salinity and stratification leads to a region of increased SSC near the limit of the salinity intrusion (Fig. 10). The increase in total SSC here is primarily due to an increase in river sediment being retained near the salinity limit, with the greatest increase occurring toward the end of neap tides when the salinity intrusion is farthest landward. This increase in SSC near the limit of the salinity intrusion varies with the strength and position of the bottom salinity front. Along the rest of the estuary, SSC decreases regardless of discharge and tidal amplitude because of the reduction in tidal amplitude and resuspension of bed sediment.

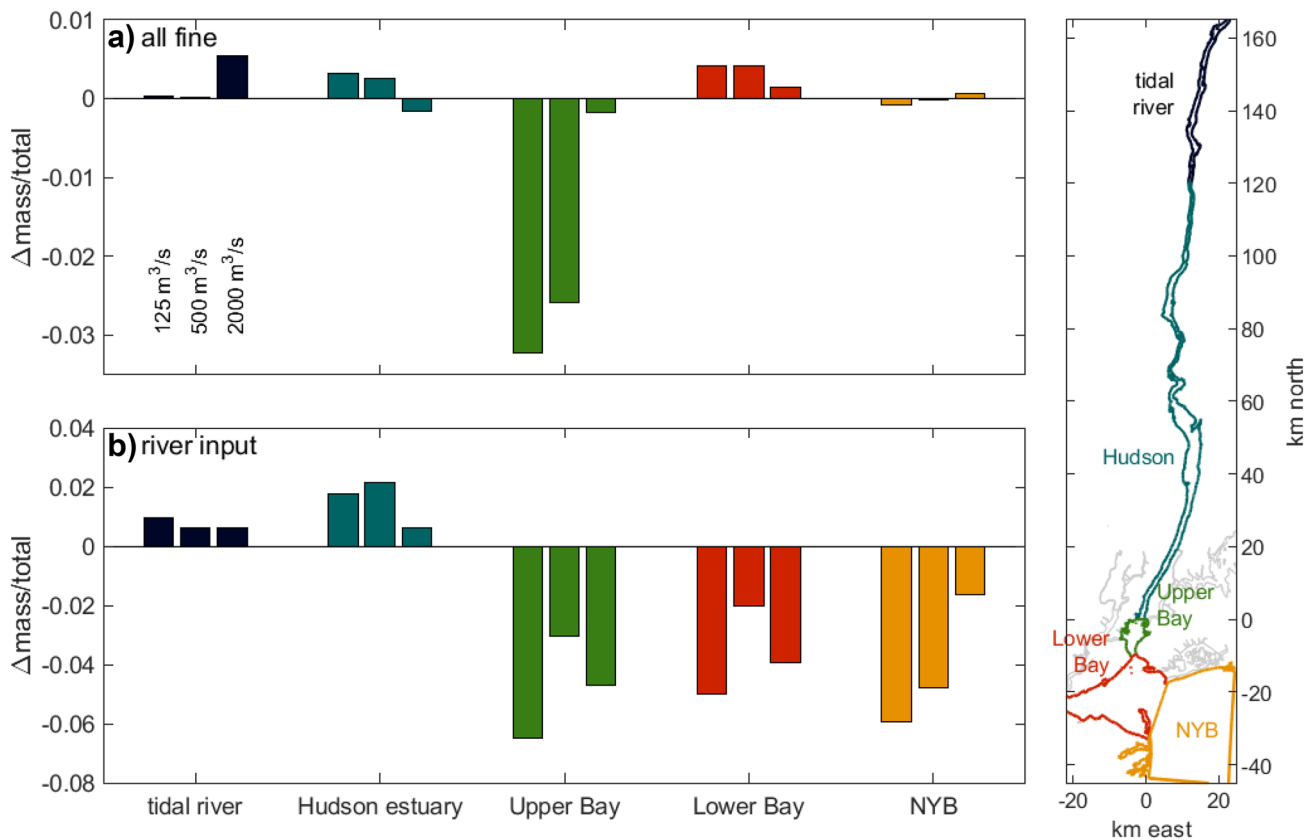


**Fig. 8** Differences in sediment mass between the base and barrier cases for different regions, as shown in panel on the right. Here, the tidal river is the region north of 120 km (extending to the tidal limit near 225 km), and the saline estuary is categorized as the region from 0 to 120 km.

**a** All fine sediment, including the initial bed and river inputs; **b** sediment input with river discharge. Differences in sediment mass for each region are shown for the discharge cases: 125, 500, and 2000  $\text{m}^3\text{s}^{-1}$

### Sediment Transport Mechanisms

Tidal velocity, bottom stress, and suspended sediment are most altered near the barrier and in the Upper Bay. Without the barrier, mean bottom stress in the channel is landward due to the estuarine circulation, and tidal stresses are slightly greater during flood tides than ebbs over most of this region (Fig. 5). The estuarine circulation can drive landward net sediment transport because SSC is greater near the bottom where the density-driven residual velocities are landward. Tidal asymmetries in velocity also drive net sediment transport due to correlations between bottom stress and SSC, with the direction of the net transport depending on the velocity asymmetry and sediment availability for resuspension (Meade 1969; Scully and Friedrichs 2007). In the Hudson ETM, an observational study found that the tidal correlations dominated the landward sediment transport and the tidal transport was greatest during spring tides and low discharge (Geyer et al. 2001). The subtidal advective flux that includes the mean flow and the estuarine circulation was generally smaller, with seaward transport during high discharge periods and spring

tides and more landward advective transport during low discharge and neaps.

The net along-estuary sediment transport in the model is compared for the three discharge cases (Fig. 11). The net transport is also decomposed with temporal and spatial averaging to quantify the contributing components: a cross-sectionally averaged and tidally filtered mean component from the river discharge and mean SSC; a tidally filtered, spatially varying steady component from the estuarine circulation and mean vertical profile of SSC; and a tidally and spatially varying component from tidal correlations in velocity and SSC (Burchard et al. 2018). Tidal variability is removed using a Godin filter (Walters and Heston 1982). The sediment flux decomposition is similar to that for salt flux in which the estuarine circulation is the dominant component of the landward salt flux in the Hudson (Lerczak et al. 2006).

The influence of the barrier on the net sediment transport is most apparent within about 10 km of the barrier for the low discharge conditions (Fig. 11a). In the base case, the total transport is generally landward through this region, with spatial variability indicating convergence and divergence and net bed sediment accumulation or loss.

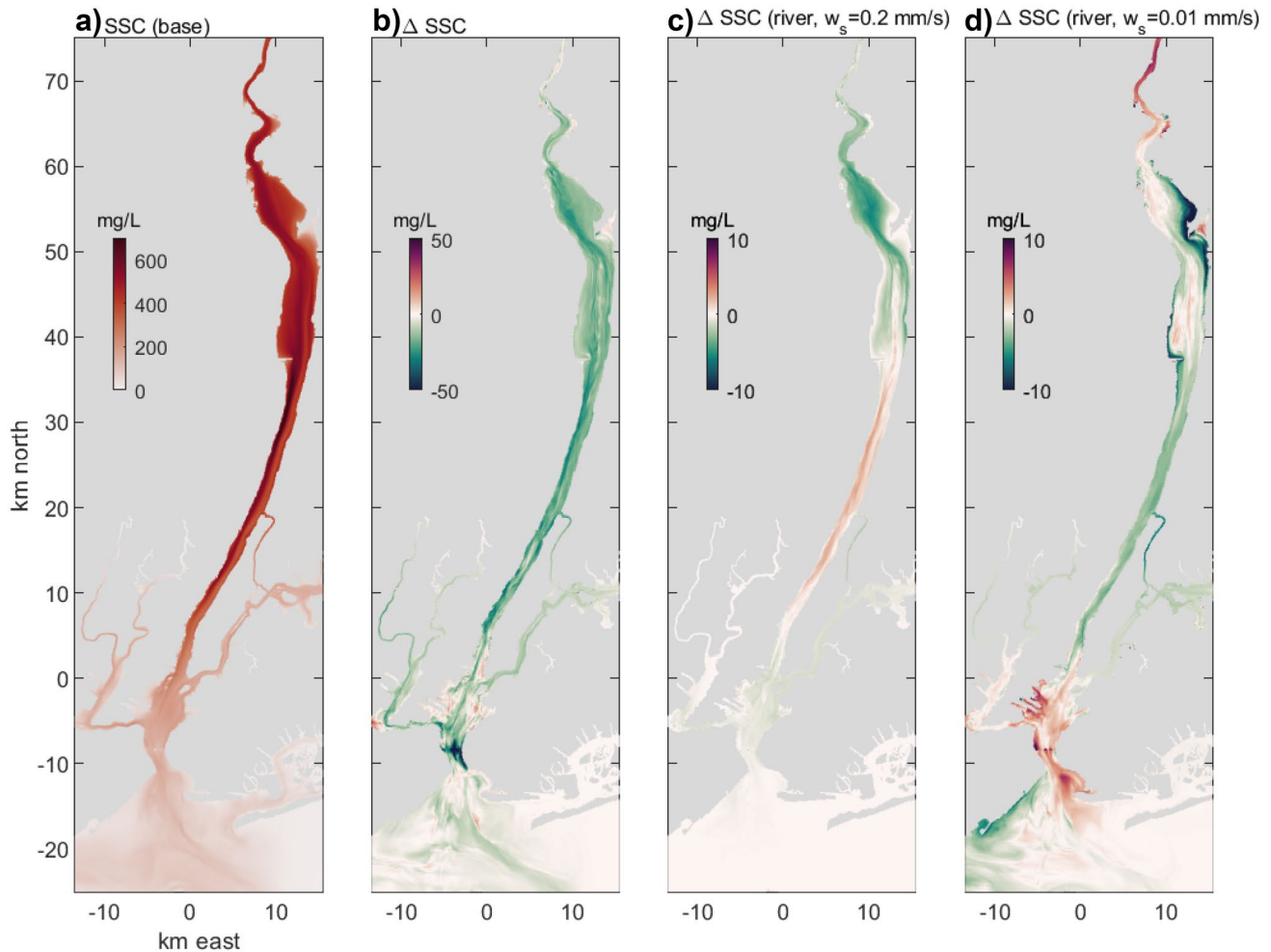


**Fig. 9** Near-bottom SSC during spring tides for  $Q_r=500 \text{ m}^3\text{s}^{-1}$  (averaged over days 32 to 34). **a** Near-bottom SSC in the base case; **b** difference between the barrier and base cases in near-bottom total SSC; **c** dif-

ference in SSC of river sediment with settling velocity ( $w_s$ )=0.2 mm/s; **d** difference in SSC of river sediment with  $w_s=0.01$  mm/s

Decomposing the total transport into its components, the mean transport is seaward due to the river outflow and the steady transport is landward due to the estuarine circulation. The tidal sediment transport is the largest term over much of the region and is the main source of spatial variability in the total. Addition of the surge barrier causes the greatest changes in this tidal transport term, and it dominates the differences in the total transport between the base and barrier cases. Landward of the barrier, the tidal sediment transport becomes more landward due to the strong velocities through barrier openings during flood tides. Seaward of the barrier, the tidal transport becomes strongly seaward due to the increased velocities through the openings during ebbs. The overall increase in tidal currents and turbulent mixing also weakens the estuarine circulation locally, and this results in a decrease in the landward steady sediment transport.

The barrier causes similar shifts in the net transport at higher discharges. In the moderate and high discharge

cases, the net transport is greater than the low flow case, it is generally seaward, and it decreases in magnitude with distance toward the mouth as sediment accumulates on the bed (Fig. 11). Correspondingly, the mean transport associated with the mean volume flux from the river decreases toward the mouth as SSC decreases downstream of the ETM. The steady circulation component is generally landward, particularly in the lower Hudson north of the Battery. The tidal sediment transport varies spatially but is generally seaward. The barrier alters the tidal component locally, making it more landward on the landward side of the barrier and more seaward on the seaward side. The remote impacts on the sediment transport inside the estuary are most apparent in the high discharge case. In the lower ETM (e.g., near 20 km north), the net seaward transport decreases with the barrier because the mean and tidal components are less seaward due to the reductions in tidal velocity and SSC.

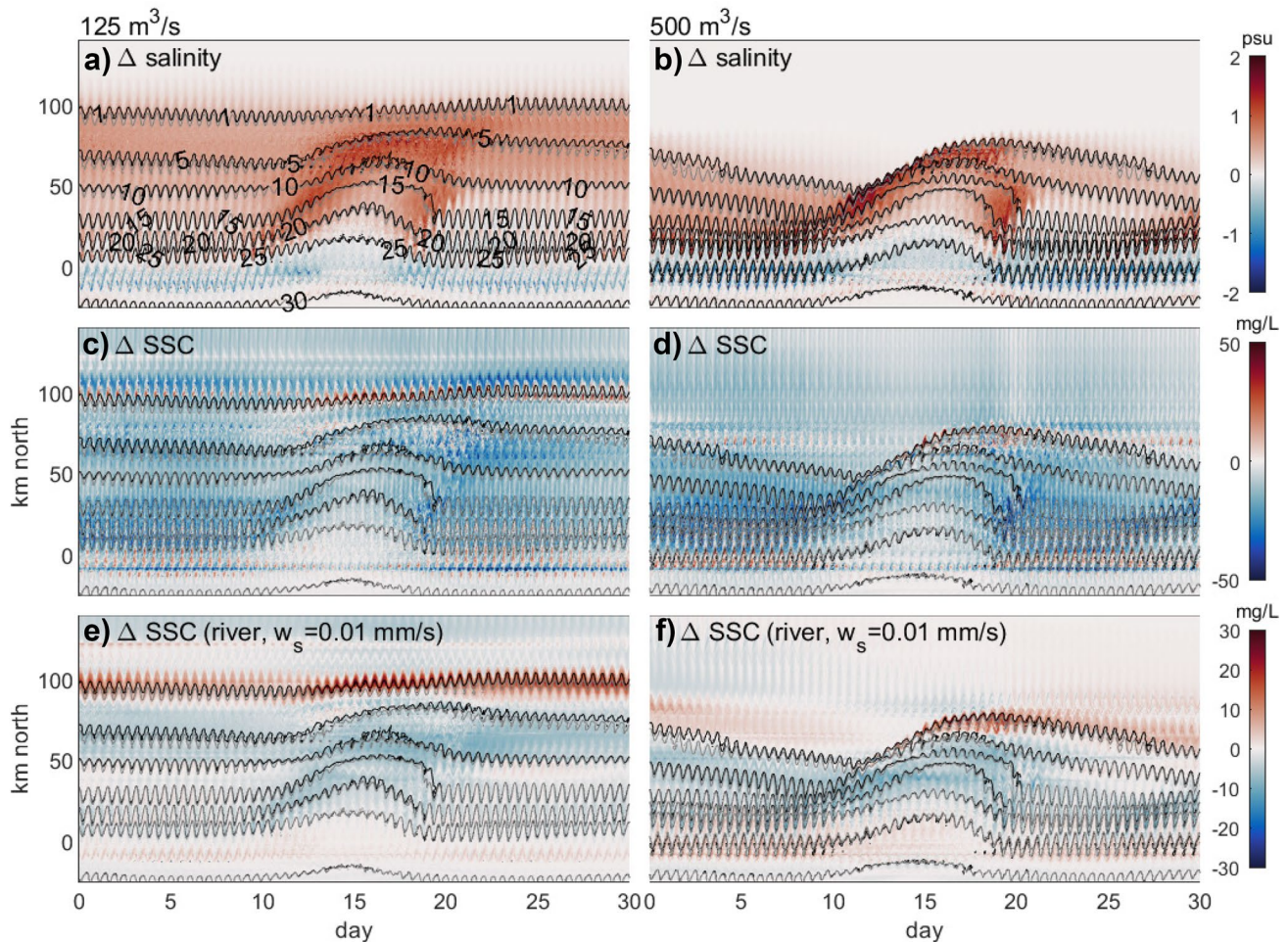


**Fig. 10** Differences in salinity and SSC with the barrier. Left panels are  $Q_r = 125 \text{ m}^3 \text{ s}^{-1}$  and right panels are  $500 \text{ m}^3 \text{ s}^{-1}$ . **a, b** Differences in near-bottom salinity between the base and barrier cases, with bottom

salinity contours for the base case; **c, d** differences in near-bottom total SSC, with bottom salinity contours; **e, f** differences in near-bottom SSC from river inputs, with bottom salinity contours

## Summary and Discussion

The direct effect of the flow constriction through barrier openings is to increase the tidal velocities both landward and seaward of the structure. The flow patterns are sharply asymmetric between flood and ebb, with jets of high velocity downstream of the openings and flow blockage upstream (Fig. 3). The tidal asymmetries in velocity result in tidal asymmetries in bottom stress (Figs. 4 and 5). The net effect is to increase seaward sediment transport seaward of the barrier and increase landward transport landward of the barrier. For moderate and high discharge conditions with the greatest watershed sediment inputs, the barrier causes increased retention of sediment in the estuary. During low discharge periods, the barrier can change the sign of the transport and reduce import of sediment from offshore. Reductions in sediment import have also been linked to the Eastern Scheldt barrier (de Vet et al. 2017). Thus, the velocity asymmetry from tidal

flow through barrier openings creates a divergence of sediment transport capacity that tends to isolate the estuary from the coastal zone. Flood-oriented velocity jets on the landward side promote retention of river inputs, and ebb-oriented jets on the seaward side reduce import from offshore.

The increased velocities near barrier openings also increase bed sediment remobilization, resulting in erosion and coarsening of the bed (Fig. 6). The reduction in availability of fine sediment for resuspension causes reductions in SSC near the barrier and in the Upper Bay. Direct influences of the barrier on bottom stress and bed sediment extend 5–10 km landward and seaward of the barrier, similar to a tidal excursion. The influence of the barrier on bed stress and SSC is greatest during low discharge periods, while for higher discharges increased mean flow and stratification reduce the direct impacts.

Reductions in tidal amplitude due to the barrier decrease sediment resuspension and increase the trapping of fine sediment

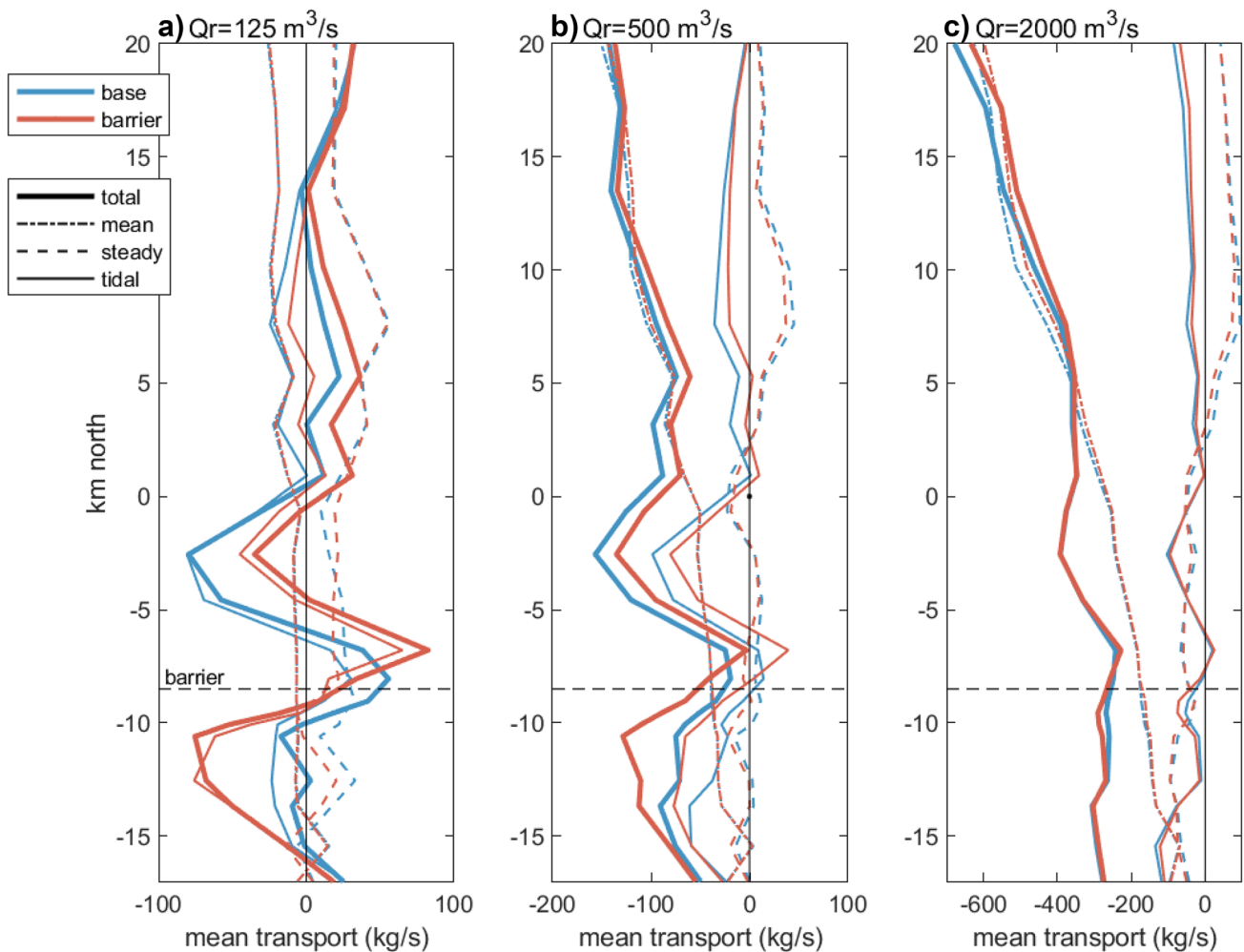


**Fig. 11** Mean sediment transport near the barrier and in lower estuary for **a**  $Q_r=125 \text{ m}^3\text{s}^{-1}$ , **b**  $500 \text{ m}^3\text{s}^{-1}$ , and **c**  $2000 \text{ m}^3\text{s}^{-1}$ , averaged over the simulation period (55 days). Each panel shows the total transport as well as the terms of the decomposition: the tidally and cross-sectionally

averaged mean component, the tidally averaged, cross-sectionally varying steady component, and the tidally and cross-sectionally varying tidal component. Barrier location is shown with a horizontal-dashed line

in the estuary (Figs. 7 and 8). In the tidal river, reductions in tidal amplitude reduce sediment resuspension and seaward transport (Wall et al. 2008; Ralston and Geyer 2017). Within the salinity intrusion, sediment trapping is increased but spatially variable (Fig. 7). Weaker tides mean stronger estuarine circulation, stronger stratification, and reduced resuspension by tidal currents, all of which tend to increase sediment trapping at bottom salinity fronts. As river discharge increases, the location of trapping shifts seaward with the salinity intrusion. Retention of river sediment in the estuary is on average a few percent greater with the barrier than without it, but locally the increase in sediment accumulation can be up to 10% depending on discharge. In the Upper Bay, retention of river sediment is reduced due to the increase in bottom stresses and bed coarsening (Figs. 7 and 8).

Despite the increase in sediment trapping, suspended sediment concentrations in the estuary decrease due to the

decrease in tidal amplitude and resuspension (Fig. 9). Over much of the estuary, the reductions in SSC with the barrier are 10% or less. As with the patterns of sediment accumulation, the differences in SSC vary with discharge and the salinity intrusion (Fig. 10). Increases in SSC from river inputs are apparent near the fresh-salt interface and in the ETM, consistent with the enhanced accumulation in those regions, but overall SSC decreases due to the reduction in tidal resuspension. The fractional reductions in SSC in the Upper Bay are around 15–30%, but for different reasons—scour from the high tidal velocities near the barrier leave less fine sediment in the bed for resuspension. Note that the bed near the barrier is likely to continue to evolve at time scales longer than the 2-month simulation period. For example, in the Eastern Scheldt scour of up to 40 m has been observed near barrier openings and the morphology continues to evolve more than three decades after barrier construction (Broekema et al. 2018).

## Potential Implications

Like many urbanized estuaries, the bed sediments of the Hudson estuary contain extensive contamination from historical industrial and municipal discharges (Olsen et al. 1993). In the Upper Bay sediments, major contaminants include PCBs, heavy metals, and PAHs (Wolfe et al. 1996; Steinberg et al. 2004; Rodenburg and Ralston 2017). The increase in bed stress near the barrier openings have the potential to remobilized contaminants adsorbed to sediment that had previously been buried below the layer of active resuspension. Remobilized sediment is likely to deposit in lower stress regions on the shoals of the Upper and Lower Bay or in the lee of the barrier structure (Fig. 6). Sediment mobilized from deeper in the bed is likely to contain higher levels of contamination than sediment presently at the surface and could potentially increase ecological risk to benthic organisms.

The reductions in SSC along the estuary could increase water clarity and potentially increase biological productivity. In the Eastern Scheldt, suspended particulate matter at a monitoring station dropped from an average of around  $300 \text{ mg L}^{-1}$  before the barrier to  $50\text{--}100 \text{ mg L}^{-1}$  afterward, and this corresponded with increases in primary productivity and benthic biomass (Brand et al. 2016). In the Hudson, the modeled decrease in SSC is less and the background sediment concentrations are greater, suggesting less impact on water clarity. The diffuse light attenuation coefficient ( $K_d$ ) in the Hudson varies seasonally, with larger  $K_d$  during the winter when higher river discharge increases SSC (Stross and Sokol 1989; Caraco et al. 1997). Light attenuation also varies spatially with values  $K_d$  of around  $1\text{--}3 \text{ m}^{-1}$  in much of the estuary and tidal river, but in the ETM  $K_d$  increases to  $5\text{--}8 \text{ m}^{-1}$  and light penetration decreases (Stross and Sokol 1989). Light attenuation scales approximately linearly with SSC in many estuaries and coastal zones including New York Bight, San Francisco Bay, Delaware Bay, and Chesapeake Bay, with a typical slope of around  $0.06 \text{ m}^{-1}/(\text{mg L}^{-1})$  (Malone 1977; Pennock 1985; Cloern 1987; Turner et al. 2021). Projected reductions in SSC of 10–20% in the Upper Bay with the barrier would correspond with similarly modest fractional increases light penetration depth. For example, assuming  $K_d = 1.5 \text{ m}^{-1}$  for summer conditions, the depth of the 1% of the surface irradiance level would increase from 3.1 to 3.7 m. In the ETM, the fractional decreases in SSC with the barrier are less and the light penetration in existing conditions is more limited, so there would be even less change in water clarity.

The decrease in SSC, in combination with the decrease in tidal amplitude and marsh inundation, could affect sediment accumulation rates in marshes and their ability to keep pace with sea level rise. For example, reductions in marsh inundation due to surge barrier closures are of concern for marsh sustainability in the Venice Lagoon (Tognin et al.

2022). Along the tidal Hudson, accretion rates in natural marshes are similar to sea level rise, and accretion rates in marshes created by anthropogenic disturbances exceed sea level rise due to the high sediment concentrations in the estuary (Yellen et al. 2021). Given these rapid accumulation rates under present conditions, the modest reductions in SSC and tidal amplitude with the barrier seem unlikely to substantially alter marsh sustainability along the Hudson.

Effects on marshes located seaward of the barrier may differ from those landward. For example in Jamaica Bay (Fig. 1), extensive marsh loss over recent decades has coincided with anthropogenic modifications including shoreline hardening, dredging of navigational channels and borrow pits, and nutrient inputs (Hartig et al. 2002; Renfro et al. 2016). Marsh sediment cores indicate that accumulation rates in Jamaica Bay are consistent with sea level rise, but the inorganic fraction has decreased compared to the pre-development era suggesting a decrease in sediment supply (Peteet et al. 2018). Local watershed inputs are minimal, so sediment supply to Jamaica Bay comes primarily from seaward sources. Estimates using multiple methods indicate that sediment supply from marine sources are less than would be needed to maintain the current marsh extent under accelerating sea level rise (Renfro et al. 2016; Chant et al. 2021). The effect of the barrier on sediment supply to Jamaica Bay was not evaluated directly because the simulations did not include wave processes that are important for sediment delivery into the bay (Hu et al. 2018; Chant et al. 2021). However, the reductions in sediment export from the Hudson into the Lower Bay and New York Bight (Fig. 8) have the potential to further reduce the sediment supply to Jamaica Bay and other coastal embayments and could further reduce marsh sustainability.

## Additional Considerations

In addition to the large barrier at the mouth of the Hudson, smaller surge barriers are being considered for Jamaica Bay and other nearby coastal embayments (US Army Corps of Engineers 2019; US Army Corps of Engineers 2021). In estuaries where sediment supply comes predominantly from seaward rather than from the local watershed, the velocity asymmetries at barrier openings and increased mixing are likely to reduce sediment import through the inlet. This reduction in transport due to the stress divergence at the barrier is in addition to any changes in export of sediment from the Hudson that may impact availability of coastal zone sediment. Alterations to sediment exchange may also depend on the design of the barrier. The fractional closure of the cross-section is the main factor affecting the increase in tidal velocities through the gates and the associated reduction in tidal amplitude, and thus affects the sediment transport. Details of the barrier design may contribute to the response,

if for example tidal lift gates with shallower depths and narrower openings result in different stress asymmetries than wider, deeper navigational openings.

Barrier closures during storm events can also affect sediment transport, depending on closure frequency and duration as well as on the conditions inside the estuary including the river discharge. In shallow embayments, feedbacks among water level, wind waves, and marsh edge erosion mean that reductions in water level during storms could cause increased marsh edge erosion (Hu et al. 2018; Tognin et al. 2022). For the Hudson barrier, waves are expected to play a minor role in sediment transport due to the relatively large water depth, strong tidal currents, natural protection from ocean swell, and limited fetch for local wave generation. However, barrier infrastructure may influence wave conditions in other estuaries where waves play a more substantial role in sediment resuspension, even during non-storm conditions. Barrier closures could also result in greater sediment trapping in the estuary due to the high discharge and sediment loading that often accompany coastal surge events. Impacts of barrier closure are not assessed here, but projections of increasing closure frequency with sea level rise (Chen et al. 2020) suggest that they could significantly influence morphological response over time.

Alterations to estuarine sediment dynamics from construction of a storm surge barrier should be considered in the context of the broader set of anthropogenic modifications (Wang et al. 2015). Sediment supply from the watershed can be altered by dam construction, flow regulation, land use changes, or trends in mean river discharge with climate change, and such factors can increase or decrease SSC and sedimentation rates (Cloern and Jassby 2012; Wang et al. 2018; Russ and Palinkas 2020). Shoreline armoring can reduce sediment inputs from wave-driven coastal erosion and cause reductions in SSC (Turner et al. 2021). Shoreline encroachment or wetland restoration can alter estuarine morphology to increase or decrease sediment availability (Klingbeil and Sommerfield 2005; Shellenbarger et al. 2013). Alterations to the tidal and salinity dynamics by dredging can increase sediment trapping in channels (Ellsworth 1986; Jalón-Rojas et al. 2016; Eidam et al. 2021) and potentially lead to hyperturbid conditions (Winterwerp et al. 2013; van Maren et al. 2015). Dredging also removes sediment from the system and can create deficits that lead to erosion and morphological adjustment (Cox et al. 2021). In the Hudson, alterations to sediment supply by dams and shoreline erosion are likely to be limited (Ellsworth 1986; Ralston et al. 2021), but dredging has, and is likely to continue to be, a factor (Panuzio 1965). For comparison, the projected landward shift in the location of the salinity intrusion with the Hudson surge barrier is similar to that from a recent dredging project that increased the navigational channel depth in the Upper Bay (Ralston 2022). However, changes in tidal

amplitude with a barrier have the opposite sense of that with dredging. Tidal amplitude generally increases with dredging and decreases with the barrier, so the impacts on SSC and sediment accumulation are likely to differ. Most estuaries that are candidates for storm surge barriers have undergone substantial modification of some kind by development, so changes resulting from a barrier should be assessed in the framework of an altered system and weighed against potential surge protection benefits.

**Supplementary Information** The online version contains supplementary material available at <https://doi.org/10.1007/s12237-023-01172-3>.

**Funding** Funding from Hudson Research Foundation (Award #003/19A).

**Data Availability** Data used in this study are available upon request.

## References

- Abood, Karim A. 1974. Circulation in the Hudson estuary. *Annals of the New York Academy of Sciences* 250: 39–111. <https://doi.org/10.1111/j.1749-6632.1974.tb43895.x>.
- Ariathurai, Ranjan, and Kandiah Arulanandan. 1978. Erosion rates of cohesive soils. *Journal of the Hydraulics Division American Society of Civil Engineers* 104: 279–283.
- Bakker, C., P.M.J. Herman, and M. Vink. 1990. Changes in seasonal succession of phytoplankton induced by the storm-surge barrier in the Oosterschelde (SW Netherlands). *Journal of Plankton Research* 12: 947–972.
- Bokuniewicz, Henry J., and Chester L. Arnold. 1984. Characteristics of suspended sediment transport in the lower Hudson River. *North-eastern Environmental Science* 3: 184–189.
- Brand, A.D., Bee Kothuis, and B. Prooijen. 2016. *The Eastern Scheldt Survey. A concise overview of the estuary pre- and post barrier. Part 2: SURVEY*. <https://doi.org/10.13140/RG.2.1.1455.5764>.
- Broekema, Y.B., R.J. Labeur, and W.S.J. Uijttewaal. 2018. Observations and analysis of the horizontal structure of a tidal jet at deep scour holes. *Journal of Geophysical Research: Earth Surface* 123: 3162–3189. <https://doi.org/10.1029/2018JF004754>.
- Burchard, Hans, Henk M. Schuttelaars, and David K. Ralston. 2018. Sediment trapping in estuaries. *Annual Review of Marine Science* 10: 371–395. <https://doi.org/10.1146/annurev-marine-010816-060535>.
- Caraco, Nina F., Jonathan J. Cole, Peter A. Raymond, David L. Strayer, Michael L. Pace, Stuart E.G. Findlay, and David T. Fischer. 1997. Zebra mussel invasion in a large, turbid river: phytoplankton response to increased grazing. *Ecology* 78: 588–602.
- Chant, Robert J., David K. Ralston, Neil K. Ganju, Cassia Pianca, Amy E. Simonson, and Richard A. Cartwright. 2021. Sediment budget estimates for a highly impacted embayment with extensive wetland loss. *Estuaries and Coasts* 44: 608–626.
- Chen, Ziyu, Philip Orton, and Thomas Wahl. 2020. Storm surge barrier protection in an era of accelerating sea-level rise: quantifying closure frequency, duration and trapped river flooding. *Journal of Marine Science and Engineering* 8: 725. <https://doi.org/10.3390/jmse8090725>.
- Cloern, James E. 1987. Turbidity as a control on phytoplankton biomass and productivity in estuaries. *Continental Shelf Research* 7: 1367–1381. [https://doi.org/10.1016/0278-4343\(87\)90042-2](https://doi.org/10.1016/0278-4343(87)90042-2).
- Cloern, James E., and Alan D. Jassby. 2012. Drivers of change in estuarine-coastal ecosystems: discoveries from four decades of study in San Francisco Bay. *Reviews of Geophysics* 50. <https://doi.org/10.1029/2012RG000397>.
- Cox, J.R., Y. Huismans, S.M. Knaake, J.R.F.W. Leuven, N.E. Vellinga, M. van der Vegt, A.J.F. Hoitink, and M.G. Kleinhans. 2021.

- Anthropogenic effects on the contemporary sediment budget of the lower Rhine-Meuse Delta Channel Network. *Earth's Future* 9: e2020EF001869. <https://doi.org/10.1029/2020EF001869>.
- de Vet, P.L.M., B.C. van Prooijen, and Z.B. Wang. 2017. The differences in morphological development between the intertidal flats of the Eastern and Western Scheldt. *Geomorphology* 281: 31–42. <https://doi.org/10.1016/j.geomorph.2016.12.031>.
- Du, Jiabi, Jian Shen, Donna M. Bilkovic, Carlton H. Hershner, and Mac Sisson. 2017. A numerical modeling approach to predict the effect of a storm surge barrier on hydrodynamics and long-term transport processes in a partially mixed estuary. *Estuaries and Coasts* 40: 387–403.
- Eelkema, Menno, Zheng B. Wang, Anneke Hibma, and Marcel J. F. Stive. 2013. Morphological effects of the Eastern Scheldt storm surge barrier on the ebb-tidal delta. *Coastal Engineering Journal* 55: 1350010-1-1350010-26. <https://doi.org/10.1142/S0578563413500101>.
- Eidam, E.F., D.A. Sutherland, D.K. Ralston, T. Conroy, and B. Dye. 2021. Shifting sediment dynamics in the Coos Bay Estuary in response to 150 years of modification. *Journal of Geophysical Research: Oceans* 126: e2020JC016771. <https://doi.org/10.1029/2020JC016771>.
- Ellsworth, John M. 1986. Sources and sinks for fine-grained sediment in the lower Hudson River. *Northeastern Geology* 8: 141–155.
- Feng, Huan, J. Kirk Cochran, David J. Hirschberg, and Robert E. Wilson. 1998. Small-scale spatial variations of natural radionuclide and trace metal distributions in sediments from the Hudson River Estuary. *Estuaries* 21: 263–280.
- Geyer, W. Rockwell., and Parker MacCready. 2014. The estuarine circulation. *Annual Review of Fluid Mechanics* 46: 175–197. <https://doi.org/10.1146/annurev-fluid-010313-141302>.
- Geyer, W. Rockwell., Jonathan D. Woodruff, and Peter Traykovski. 2001. Sediment transport and trapping in the Hudson River Estuary. *Estuaries* 24: 670–679.
- Haidvogel, D.B., H. Arango, W.P. Budgell, B.D. Cornuelle, E. Curchitser, E. Di Lorenzo, K. Fennel, et al. 2008. Ocean forecasting in terrain-following coordinates: Formulation and skill assessment of the Regional Ocean Modeling System. *Journal of Computational Physics* 227: 3595–3624. <https://doi.org/10.1016/j.jcp.2007.06.016>.
- Hartig, Ellen Kraeuer, Vivien Gornitz, Alexander Kolker, Frederick Mushacke, and David Fallon. 2002. Anthropogenic and climate-change impacts on salt marshes of Jamaica Bay, New York City. *Wetlands* 22: 71–89.
- Hu, Kelin, Qin Chen, Hongqing Wang, Ellen K. Hartig, and Philip M. Orton. 2018. Numerical modeling of salt marsh morphological change induced by Hurricane Sandy. *Coastal Engineering* 132: 63–81.
- Jalón-Rojas, Isabel, Sabine Schmidt, Aldo Sottolichio, and Christine Bertier. 2016. Tracking the turbidity maximum zone in the Loire Estuary (France) based on a long-term, high-resolution and high-frequency monitoring network. *Continental Shelf Research* 117: 1–11. <https://doi.org/10.1016/j.csr.2016.01.017>.
- Klingbeil, Andrew D., and Christopher K. Sommerfield. 2005. Latest Holocene evolution and human disturbance of a channel segment in the Hudson River Estuary. *Marine Geology* 218: 135–153. <https://doi.org/10.1016/j.margeo.2005.02.026>.
- Lerczak, James A., W. Rockwell Geyer, and Robert J. Chant. 2006. Mechanisms Driving the time-dependent salt flux in a partially stratified estuary. *Journal of Physical Oceanography* 36: 2296–2311.
- Malone, Thomas C. 1977. Environmental regulation of phytoplankton productivity in the lower Hudson estuary. *Estuarine and Coastal Marine Science* 5: 157–171.
- Meade, Robert H. 1969. Landward transport of bottom sediments in estuaries of the Atlantic Coastal Plain. *Journal of Sedimentary Petrology* 39: 222–234.
- Mooyaart, L.F., and S.N. Jonkman. 2017. Overview and design considerations of storm surge barriers. *Journal of Waterway, Port, Coastal, and Ocean Engineering* 143: 06017001. [https://doi.org/10.1061/\(ASCE\)WW.1943-5460.0000383](https://doi.org/10.1061/(ASCE)WW.1943-5460.0000383).
- Nicholls, Robert John, Jochen Hinkel, Daniel Lincke, and Thomas van der Pol. 2019. Global investment costs for coastal defense through the 21st century. *World Bank Policy Research Working Paper* 8745.
- Nienhuis, P.H., and A.C. Smaal. 1994. The Oosterschelde estuary, a case-study of a changing ecosystem: an introduction. *Hydrobiologia* 282: 1–14. [https://doi.org/10.1007/978-94-011-1174-4\\_1](https://doi.org/10.1007/978-94-011-1174-4_1).
- Nitsche, F.O., W.B.F. Ryan, S.M. Carbotte, R.E. Bell, A. Slagle, C. Bertinado, R. Flood, T. Kenna, and C. McHugh. 2007. Regional patterns and local variations of sediment distribution in the Hudson River Estuary. *Estuarine, Coastal and Shelf Science* 71: 259–277. <https://doi.org/10.1016/j.ecss.2006.07.021>.
- Nitsche, F.O., T.C. Kenna, and M. Haberman. 2010. Quantifying 20th century deposition in complex estuarine environment: An example from the Hudson River. *Estuarine, Coastal and Shelf Science* 89: 163–174. <https://doi.org/10.1016/j.ecss.2010.06.011>.
- Olsen, Curtis R., H.J. Simpson, R.F. Bopp, S.C. Williams, T.H. Peng, and B.L. Deck. 1978. A geochemical analysis of the sediments and sedimentation in the Hudson Estuary. *Journal of Sedimentary Research* 48: 401–418.
- Olsen, Curtis R., Ingvar L. Larsen, Patrick J. Mulholland, Karen L. von Damm, Jacqueline M. Grebmeier, Linda C. Schaffner, Robert J. Diaz, and Maynard M. Nichols. 1993. The concept of an equilibrium surface applied to particle sources and contaminant distributions in estuarine sediments. *Estuaries* 16: 683–696.
- Orton, Philip M., T.M. Hall, S.A. Talke, A.F. Blumberg, N. Georgas, and S. Vinogradov. 2016. A validated tropical-extratropical flood hazard assessment for New York Harbor. *Journal of Geophysical Research: Oceans* 121: 8904–8929. <https://doi.org/10.1002/2016JC011679>.
- Panuzio, F.L. 1965. Lower Hudson River siltation. In *Proceedings of the 2nd Federal Interagency Sedimentation Conference*, 512–550. Misc. Publication 970. Jackson, MS: Agricultural Research Service.
- Pennock, Jonathan R. 1985. Chlorophyll distributions in the Delaware estuary: regulation by light-limitation. *Estuarine, Coastal and Shelf Science* 21: 711–725.
- Peteet, Dorothy M., Jonathan Nichols, Timothy Kenna, Clara Chang, James Browne, Mohammad Reza, Stephen Kovari, Louisa Liberman, and Stephanie Stern-Protz. 2018. Sediment starvation destroys New York City marshes' resistance to sea level rise. *Proceedings of the National Academy of Sciences* 115: 10281–10286.
- Postma, H. 1967. Sediment transport and sedimentation in the estuarine environment. In *Estuaries*, 83: 158–179. Washington, DC: American Association for the Advancement of Science.
- Ralston, David K., and W. Rockwell Geyer. 2009. Episodic and long-term sediment transport capacity in the Hudson River Estuary. *Estuaries and Coasts* 32: 1130–1151. <https://doi.org/10.1007/s12237-009-9206-4>.
- Ralston, David K., and W. Rockwell Geyer. 2017. Sediment transport time scales and trapping efficiency in a tidal river. *Journal of Geophysical Research: Earth Surface* 122: 2042–2063.
- Ralston, David K., W. Rockwell Geyer, and James A. Lerczak. 2008. Subtidal salinity and velocity in the Hudson River Estuary: Observations and modeling. *Journal of Physical Oceanography* 38: 753–770.
- Ralston, David K., W. Rockwell Geyer, and John C. Warner. 2012. Bathymetric controls on sediment transport in the Hudson River estuary: Lateral asymmetry and frontal trapping. *Journal of Geophysical Research* 117: C10013. <https://doi.org/10.1029/2012JC008124>.
- Ralston, David K., John C. Warner, W. Rockwell Geyer, and Gary R. Wall. 2013. Sediment transport due to extreme events: the Hudson River estuary after tropical storms Irene and Lee. *Geophysical Research Letters* 40: 2013GL057906. <https://doi.org/10.1002/2013GL057906>.

- Ralston, David K., Brian Yellen, and Jonathan D. Woodruff. 2021. Watershed sediment supply and potential impacts of dam removals for an estuary. *Estuaries and Coasts* 44: 1195–1215. <https://doi.org/10.1007/s12237-020-00873-3>.
- Ralston, David K. 2022. Impacts of storm surge barriers on drag, mixing, and exchange flow in a partially mixed estuary. *Journal of Geophysical Research: Oceans*. Wiley Online Library: e2021JC018246.
- Renfro, Alisha A., J. Kirk Cochran, David J. Hirschberg, Henry J. Bokuniewicz, and Steven L. Goodbred Jr. 2016. The sediment budget of an urban coastal lagoon (Jamaica Bay, NY) determined using <sup>234</sup>Th and <sup>210</sup>Pb. *Estuarine, Coastal and Shelf Science* 180: 136–149.
- Rodenburg, Lisa A., and David K. Ralston. 2017. Historical sources of polychlorinated biphenyls to the sediment of the New York/New Jersey Harbor. *Chemosphere* 169: 450–459. <https://doi.org/10.1016/j.chemosphere.2016.11.096>.
- Russ, Emily, and Cindy Palinkas. 2020. Evolving sediment dynamics due to anthropogenic processes in upper Chesapeake Bay. *Estuarine, Coastal and Shelf Science* 235: 106596.
- Scully, Malcolm E., and Carl T. Friedrichs. 2007. Sediment pumping by tidal asymmetry in a partially mixed estuary. *Journal of Geophysical Research* 112: 12. <https://doi.org/10.1029/2006JC003784>.
- Shchepetkin, Alexander F., and James C. McWilliams. 2005. The regional oceanic modeling system (ROMS): A split-explicit, free-surface, topography-following-coordinate oceanic model. *Ocean Modelling* 9: 347–404. <https://doi.org/10.1016/j.ocemod.2004.08.002>.
- Shellenbarger, Gregory G., Scott A. Wright, and David H. Schoellhamer. 2013. A sediment budget for the southern reach in San Francisco Bay, CA: implications for habitat restoration. *Marine Geology* 345: 281–293.
- Slagle, A.L., W.B.F. Ryan, S.M. Carbotte, R. Bell, F.O. Nitsche, and T. Kenna. 2006. Late-stage estuary infilling controlled by limited accommodation space in the Hudson River. *Marine Geology* 232: 181–202. <https://doi.org/10.1016/j.margeo.2006.07.009>.
- Sommerfield, Christopher K. 2006. On sediment accumulation rates and stratigraphic completeness: Lessons from Holocene ocean margins. *Continental Shelf Research* 26: 2225–2240. <https://doi.org/10.1016/j.csr.2006.07.015>.
- Steinberg, Nancy, Dennis J. Suszkowski, Lori Clark, and Juliette Way. 2004. Health of the harbor. *The first comprehensive look at the State of the NY/NJ Harbor estuary. A report to the NY/NJ Harbor Estuary Program*. New York, NY: Hudson River Foundation.
- Strauss, Benjamin H., Philip M. Orton, Klaus Bittermann, Maya K. Buchanan, Daniel M. Gilford, Robert E. Kopp, Scott Kulp, Chris Massey, Hans de Moel, and Sergey Vinogradov. 2021. Economic damages from Hurricane Sandy attributable to sea level rise caused by anthropogenic climate change. *Nature Communications* 12: 2720. <https://doi.org/10.1038/s41467-021-22838-1>.
- Stross, R.G., and R.C. Sokol. 1989. Runoff and flocculation modify underwater light environment of the Hudson River Estuary. *Estuarine, Coastal and Shelf Science* 29: 305–316. [https://doi.org/10.1016/0272-7714\(89\)90030-9](https://doi.org/10.1016/0272-7714(89)90030-9).
- Talke, Stefan A., Philip Orton, and David A. Jay. 2014. Increasing storm tides in new york harbor, 1844–2013. *Geophysical Research Letters* 41: 3149–3155.
- Ten Brinke, Wilfried, Job Dronkers, and Jan PM Mulder. 1994. Fine sediments in the Oosterschelde tidal basin before and after partial closure. In *The Oosterschelde Estuary (The Netherlands): a Case-Study of a Changing Ecosystem*, 41–56. Springer.
- Tognin, Davide, Alvise Finotello, Andrea D'Alpaos, Daniele P. Viero, Mattia Pivato, Riccardo A. Mel, Andrea Defina, Enrico Bertuzzo, Marco Marani, and Luca Carniello. 2022. Loss of geomorphic diversity in shallow tidal embayments promoted by storm-surge barriers. *Science Advances* 8: eabm8446.
- Traykovski, Peter, W. Rockwell Geyer, and Chris Sommerfield. 2004. Rapid sediment deposition and fine-scale strata formation in the Hudson estuary. *Journal of Geophysical Research* 109: F02004. <https://doi.org/10.1029/2003JF000096>.
- Turner, Jessica S., Pierre St-Laurent, Marjorie A. M. Friedrichs, and Carl T. Friedrichs. 2021. Effects of reduced shoreline erosion on Chesapeake Bay water clarity. *Science of The Total Environment* 769: 145157. <https://doi.org/10.1016/j.scitotenv.2021.145157>.
- US Army Corps of Engineers. 2019. *New York – New Jersey Harbor and Tributaries Coastal Storm Risk Management Feasibility Study - Overview of Engineering Work for the NYNJHATS Interim Report*.
- US Army Corps of Engineers, Philadelphia District. 2021. *New Jersey Back Bays Coastal Storm Risk Management Draft Integrated Feasibility Report and Tier 1 Environmental Impact Statement*.
- van Maren, D.S., T. van Kessel, K. Cronin, and L. Sittoni. 2015. The impact of channel deepening and dredging on estuarine sediment concentration. *Continental Shelf Research* 95: 1–14. <https://doi.org/10.1016/j.csr.2014.12.010>.
- Wall, G., E. Nystrom, and S. Litten. 2008. Suspended sediment transport in the freshwater reach of the Hudson River Estuary in eastern New York. *Estuaries and Coasts*. <https://doi.org/10.1007/s12237-008-9050-y>.
- Walters, Roy A., and Cynthia Heston. 1982. Removing tidal-period variations from time-series data using low-pass digital filters. *Journal of physical oceanography* 12: 112–115.
- Wang, Z.B., D.S. Van Maren, P.X. Ding, S.L. Yang, B.C. Van Prooijen, P.L.M. De Vet, J.C. Winterwerp, H.J. De Vriend, M.J.F. Stive, and Q. He. 2015. Human impacts on morphodynamic thresholds in estuarine systems. *Continental Shelf Research* 111: 174–183. <https://doi.org/10.1016/j.csr.2015.08.009>.
- Wang, Chongyang, Weijiao Li, Shuisen Chen, Dan Li, Danni Wang, and Jia Liu. 2018. The spatial and temporal variation of total suspended solid concentration in Pearl River Estuary during 1987–2015 based on remote sensing. *Science of the Total Environment* 618: 1125–1138. <https://doi.org/10.1016/j.scitotenv.2017.09.196>.
- Warner, John C., Christopher R. Sherwood, Richard P. Signell, Courtney K. Harris, and Hernan G. Arango. 2008. Development of a three-dimensional, regional, coupled wave, current, and sediment-transport model. *Computers & Geosciences* 34: 1284–1306. <https://doi.org/10.1016/j.cageo.2008.02.012>.
- Winterwerp, Johan C., Zheng Bing Wang, Alexander van Braeckel, Gijsbert van Holland, and Frank Kösters. 2013. Man-induced regime shifts in small estuaries—II: A comparison of rivers. *Ocean Dynamics* 63: 1293–1306. <https://doi.org/10.1007/s10236-013-0663-8>.
- Wolfe, Douglas, Edward Long, and Glen Thursby. 1996. Sediment toxicity in the Hudson-Raritan estuary: Distribution and correlations with chemical contamination. *Estuaries and Coasts* 19: 901–912. <https://doi.org/10.1007/BF02690400>.
- Woodruff, Jonathan D., W. Rockwell Geyer, Christopher K. Sommerfield, and Neal W. Driscoll. 2001. Seasonal variation of sediment deposition in the Hudson River estuary. *Marine Geology* 179: 105–119. [https://doi.org/10.1016/S0025-3227\(01\)00182-7](https://doi.org/10.1016/S0025-3227(01)00182-7).
- Yellen, Brian, Jonathan Woodruff, Caroline Ladlow, David K. Ralston, Sarah Fernald, and Waverly Lau. 2021. Rapid tidal marsh development in anthropogenic backwaters. *Earth Surface Processes and Landforms* 46: 554–572.

Springer Nature or its licensor (e.g. a society or other partner) holds exclusive rights to this article under a publishing agreement with the author(s) or other rightsholder(s); author self-archiving of the accepted manuscript version of this article is solely governed by the terms of such publishing agreement and applicable law.